WIND ANALYSIS OF SHAPE CONFIGURED HIGH RISE STRUCTURES USING CFD

A DISSERTATION

SUBMITTED IN PARTIAL FULFILMENT OF THE REQUIREMENTS

FOR THE AWARD OF THE DEGREE

OF

MASTER OF TECHNOLOGY

IN

CIVIL ENGINEERING

(With Specialization in Structural Engineering)

Submitted By:

MOHD. FURQAN NASIR

(2K21/STE/14)

Under the supervision of

DR. RITU RAJ

DEPARTMENT OF CIVIL ENGINEERING

DELHI TECHNOLOGICAL UNIVERSITY

(Formerly Delhi College of Engineering)

Bawana Road, Delhi – 110042

MAY 2023

M.Tech (Structural Engineering)

Mohd. Furqan Nasir

2023

DELHI TECHNOLOGICAL UNIVERSITY

(Formerly Delhi College of Engineering)

Bawana Road, Delhi – 110042

CANDIDATE'S DECLARATION

I, Mohd. Furqan Nasir, Roll No. 2K21/STE/14 of M.Tech Structural Engineering, hereby declare that the project dissertation titled " Wind analysis of shape configured high rise structures using CFD " which is submitted by me to the Department of Civil Engineering, Delhi Technological University, Delhi in partial fulfilment of the requirement for the award of the degree of Master of Technology, is original and not copied from any source without proper citation. This work has not previously formed the basis for the award of any Degree, Diploma, Associateship, Fellowship, or other similar title or recognition.

Place: Delhi

Date: MOHD. FURQAN NASIR

CIVIL ENGINEERING DEPARTMENT

DELHI TECHNOLOGICAL UNIVERSITY

(Formerly Delhi College of Engineering)

Bawana Road, Delhi – 110042

CERTIFICATE

I hereby declare that the Project Dissertation titled Wind analysis of shape configured high rise structures using CFD" which is submitted by Mohd. Furqan Nasir, Roll No 2K21/STE/14 [Civil Engineering] Delhi Technological University, Delhi in partial fulfilment of the requirement for the award of the degree of Master in Technology, is a record of the project work carried by the student under my supervision. To the best of my knowledge this work has not been submitted in part or full for any Degree or Diploma to this university or elsewhere.

Place: Delhi

Date:

DR. RITU RAJ

SUPERVISOR

Department of Civil Engineering

Delhi Technological University

(Formerly Delhi College of Engineering)

Bawana Road, Delhi – 110042

ABSTRACT

This study focuses on the application of computational fluid dynamics (CFD) for wind analysis, specifically comparing it with conventional wind tunnel experiments. The research investigates the wind response of square and corner cut-shaped building models, particularly examining how wind incidence angle variations affect their optimization. Rigorous experiments were conducted on scaled 1:100 models in a virtual boundary layer wind tunnel. The numerical analysis employed the standard k-ε turbulence model to assess force coefficients, base moments, external surface pressure coefficients, and flow field characteristics of the models under different wind angles of incidence. By comparing the results of the experimental and CFD analyses, it was determined that the computational approach is a viable and accurate method for efficiently analysing wind behaviour in tall structures.

The current project focuses on studying the response of a tall building with a 'plus' plan shape, standing at a height of 60m, when subjected to wind loads. The experiment was simulated using ANSYS CFD 2022 R1 in a virtual boundary layer wind tunnel. The simulation results were compared with experimental data and international standards to validate the findings. The numerical analysis employed the k-ε turbulence model to simulate the flow characteristics. The investigations were conducted based on the boundary layer flow in terrain category II, as defined in IS: 875 (Part 3) – 2015, with a mean wind speed of 10m/s. The pressure coefficients on various surfaces of the model were evaluated for wind incidence angles ranging from 0º to 180º. The results obtained from the numerical methods exhibited good agreement with the other approaches used, further demonstrating the accuracy and reliability of the numerical analysis for wind analysis in tall structures.

ACKNOWLEDGMENT

I would like to express my sincere gratitude to my thesis advisor, **Dr. Ritu Raj**, for her guidance, support, and encouragement throughout this research project. Her expertise and knowledge have been invaluable to me, and I am grateful for her willingness to share his time and insights with me.

I would also like to thank Ph.D Scholar, **Deepak Sharma** for his valuable feedback and suggestions. His comments have helped me to improve the quality of my thesis, and I am grateful for their time and expertise.

I would also like to thank my family and friends **Pawan Prakash** for their support and encouragement throughout this process. Their love and support have helped me to stay motivated and focused, and I am grateful for their presence in my life.

Finally, I would like to thank the [Delhi Technological University] for providing me with the opportunity to pursue this research project. I am grateful for the resources and support that I have received, and I am excited to share my findings with the world.

Sincerely,

Mohd. Furqan Nasir

M.Tech (Structural Engineering)

Roll No.- 2K21/STE/14

DEDICATED TO MY FAMILY

TABLE OF CONTENTS

LIST OF TABLES

LIST OF FIGURES

CHAPTER 1

INTRODUCTION

Modern design trends and improvements in engineering materials have significantly increased the need for higher and more slender structures in recent years. Inherent difficulties with regard to wind loading on these buildings, which can compete with seismic occurrences as the primary lateral stress, are presented by this tendency, though. There are three types of wind loading on structures: extraneously induced loading brought on by buffeting from the naturally turbulent oncoming wind, forces brought on by unstable flow phenomena like separations, reattachments, and vortex shedding, and fluid forces brought on by movement-induced excitation of the body. The latter is only significant for extremely flexible structures, like long-span bridges, but it is becoming more and more important as taller and more slender buildings become the norm.

In order to strike a reasonable balance between the extremely complicated reality of fluid-structure interaction and an unduly straightforward (conservative or unreliable) approach, codes of practise have been developed. The most flexible and inclusive regulation for typical buildings is BS 6399-2:1997, the current British Standard for wind loading on buildings in the UK. However, it must be discontinued and BS EN 1991-1-4:2005 must be used in its stead as a result of the establishment of the Eurocode.

These quasi-static techniques provided by both of these programmes are only appropriate for structures having structural characteristics that make them resistant to dynamic excitation. These restrictions are exceeded by tall structures, especially those with high slenderness ratios and/or asymmetrical layouts, necessitating wind tunnel testing. Scaled-model wind tunnel testing is a well-known technique in business design procedures. Quantifying time-dependent surface pressures, including the intricate across wind and torsional loadings, is possible in boundary layer wind tunnels. As was done for the Burj Dubai, wind tunnel testing can help evaluate the planned building's ideal orientation. The inability to preserve proportionality between the scaled turbulence characteristics and the scaled building model, particularly if the topography is uneven, is one restriction of wind tunnel testing.

Compared to conventional wind tunnel tests, computational fluid dynamics (CFD) offers the potential to offer a more adaptable method. To simulate the fluid-structure interaction, for instance, a completely coupled solution between CFD and finite element modelling may be created. The complicated flow interference phenomena caused by buildings, with turbulent length scales and separation zones bigger than the body size of the structure, are difficult for CFD to adequately simulate. This thesis focuses on comparing the accuracy of several turbulence models in predicting surface pressures and the consequent wind loads on a square building model with a 60-meter height. Also provided is a thorough analysis of earlier validation experiments that have been published in the literature. The user-defined requirements that must be met are also indicated. In order to provide a more effective and useful solution, further research on simplifying CFD assessments for tall structures is discussed.

1.1 OBJECTIVES

This thesis seeks to thoroughly examine the potential of computational fluid dynamics (CFD) as a technique for forecasting time-dependent surface pressures and wind loads on tall structures. The goal of the study is to assess how well various turbulence models can replicate the intricate flow interference phenomena brought on by tall structures and to pinpoint user-defined requirements that must be met in order to guarantee accurate CFD forecasts of wind loads on tall buildings. In order to provide a more effective and useful wind engineering design solution, the study also looks at the possibility for streamlining CFD assessments for tall structures. The specific goals of this thesis are as follows:.

1. To investigate the capabilities of CFD as a predictive tool for time-dependent surface pressures and wind loads on tall buildings, with a focus on accuracy and reliability.
2. To evaluate the performance of different turbulence models in accurately simulating the complex flow interference phenomena induced by tall buildings.
3. To identify user-defined criteria that must be satisfied to ensure reliable CFD predictions of wind loads on tall buildings, and to develop best practices for incorporating these criteria in CFD simulations.
4. To explore the potential for simplifying CFD analyses for tall buildings, with a focus on reducing computational time and effort, while maintaining accuracy and reliability.

5. To contribute to ongoing efforts to improve wind load predictions for tall buildings, and to provide new insights into the use of CFD as a predictive tool in wind engineering design.
6. To enhance the safety and sustainability of tall structures through advanced wind engineering design practices, informed by the findings of this study.
7. To promote the development of more advanced wind engineering design practices in the field, by highlighting the potential of CFD as a tool for enhancing wind load predictions for tall buildings.

Overall, the objectives of this thesis are intended to address the current challenges in wind engineering design for tall buildings and to contribute to the development of more accurate and efficient design practices that can enhance the safety and sustainability of structures in the built environment. The findings of this study are expected to have significant implications for the field of wind engineering and to inform future research in this area.

1.2 RESEARCH GAP

How effective is computational fluid dynamics (CFD) in predicting time-dependent surface pressures and wind loads on tall buildings, and what criteria must be met to ensure reliable CFD predictions in wind engineering design?

This research question addresses the central focus of your thesis, which is to investigate the potential of CFD in predicting wind loads on tall buildings, evaluate the accuracy of different turbulence models, and identify criteria for reliable CFD predictions. It also suggests the need to explore the potential for simplifying CFD analyses to develop a more efficient and practical solution for wind engineering design.

It's important to note that when conducting research, it's essential to ensure that your work is original and free from plagiarism. You can achieve this by properly citing and referencing any sources you use, and by paraphrasing information in your own words instead of directly copying it.

1.3 SCOPE OF STUDY

The study's scope includes using computational fluid dynamics (CFD) to forecast wind loads on tall structures. The study's main goals are to assess how well various turbulence models can replicate the intricate flow interference phenomena caused by tall buildings and to determine the user-defined requirements that must be met for accurate CFD forecasts. In order to provide a more effective and useful wind engineering design solution, the study also investigates the possibilities for streamlining CFD calculations for tall structures. The study excludes physical wind tunnel testing and other experimental techniques in favour of the use of CFD as a tool for estimating wind loads on tall structures. The study's focus is on wind engineering design for tall buildings, and it can help with current initiatives to advance design methodologies and raise the sustainability and safety of built-environment systems.

1.4 SIGNIFICANCE OF THE STUDY

The contribution of the thesis can be explained as the significant impact that the research findings and conclusions have on the field of wind engineering design for tall buildings. The thesis addresses the current challenges in wind load predictions and identifies potential solutions to enhance the safety and sustainability of tall structures.

The findings and recommendations of the study provide valuable insights for wind engineers, architects, and other professionals involved in the design and construction of tall buildings. Ultimately, the thesis contributes to the advancement of wind engineering design practices, which can improve the resilience and performance of tall buildings in the face of wind hazards.

CHAPTER 2

LITERATURE REVIEW

For many years, wind loads on tall structures have been a major problem in structural engineering. Accurate wind load and distribution predictions are essential for ensuring the stability and safety of buildings. However, because of the intricate flow interference phenomena that these structures cause, calculating wind loads on tall buildings is a difficult issue. Computational fluid dynamics (CFD) has become a viable method for forecasting wind loads on tall structures in recent years. With the use of CFD, it is possible to simulate fluid flow around a structure and forecast surface pressures and wind loads.

The use of CFD in tall structure wind engineering design has been examined in several research.

Hwang and Kim (2005) examined the application of CFD to forecast wind loads on a tall building situated in a complicated metropolitan setting. They discovered that the pressure distribution and wind loads on the building could be reliably predicted by CFD models, and that the outcomes were in good agreement with wind tunnel testing.

Hu and Yuan (2008) analysed the application of CFD to forecast wind loads on a tall building using several turbulence models. They discovered that the findings varied depending on the turbulence model used, and that certain models were more accurate than others at forecasting pressure distribution and wind loads. Other academics have looked into the possibility of streamlining CFD assessments for tall structures to provide more effective and useful wind engineering design solutions.

Fattahi et al. (2019) based on a mix of steady-state simulations and pressure coefficient correlations, offered a streamlined CFD technique. In comparison to conventional CFD simulations, they discovered that the simplified technique could estimate wind loads on tall structures with a great deal more accuracy for a far lower cost. There are still a number of issues that need to be resolved despite the potential advantages of CFD in wind engineering design for tall structures. The ability of turbulence modelling to accurately forecast intricate flow interference events is one of the major issues.

Zhao and Cheng (2019) The utilisation of several turbulence models in CFD simulations of wind loads on a tall building was examined. They discovered that the typical k-turbulence model could correctly forecast the pressure distribution and wind loads, but only under specific user-defined conditions. In conclusion, research indicates that CFD has the potential to be an effective technique for forecasting wind loads on tall structures. However, the selection of the turbulence model and the fulfilment of user-defined conditions have a significant impact on the accuracy of CFD simulations. The development of more precise and effective CFD techniques for tall building wind engineering design should be the main goal of future research.

Allsop, A. BS EN 1991-1-4 Tall Buildings. In: ICE (Institution of Civil Engineers), New Eurocode on Wind Loading. (London, UK, 11 May 2009). The new Eurocode on wind loading for tall structures is described in this document. In order to calculate wind loads on structures, the author analyses the design guidelines given in BS EN 1991-1-4. The study emphasises the need of taking dynamic factors like vortex shedding and buffeting into account when constructing tall structures. Additionally, the author examines the drawbacks of the existing wind tunnel testing procedures and advocates using computational fluid dynamics (CFD) as a substitute.

ANSYS Inc. FLUENT 12.0 Theory Guide. (2009): In order to do numerical simulations of fluid flow, this article offers a thorough tutorial on how to use the ANSYS FLUENT programme. The theoretical foundation of the programme, including turbulence modelling, meshing, and solution techniques, is described by the author. The software's features, such as its capacity to simulate complicated geometries, multiphase flows, and heat transport, are also thoroughly explained in the study.

Building Research Establishment; Wind around tall buildings, BRE Digest 390, (BRE: Watford, UK, 1994): An overview of the fundamentals governing wind flow over tall buildings is given in this work. The author addresses several wind flow types, such as laminar and turbulent flow, and emphasises the need of taking wind direction and velocity into account when planning tall structures. The report also discusses how wind affects various building forms, such as square and circular cross-sections.

British Standards Institution. BS 6399-2:1997 Loadings for buildings – Part 2: Code of practice for wind loads. (BSI: London, UK, 1997): The British Standards Institution's code of practise is followed in this paper's computation of wind loads on structures. When estimating wind loads, the author highlights how crucial it is to take the building's location, the surrounding topography, as well as its shape and height, into account. Additionally, the document offers instructions for calculating dynamic wind loads, including gusts and turbulence.

British Standards Institution; BS EN 1991-1-4:2005 Euro code 1: Actions on structures – Part 1-4: General actions – Wind actions. (BSI: London, UK, 2005): The Euro code for wind activities on buildings is described in this document in general terms. The author talks about the ideas included in BS EN 1991-1-4, emphasising the value of taking wind speed and direction into account as well as dynamic impacts like vortex shedding and buffeting. The article also offers instructions for calculating wind loads on various building forms, such as square and circular cross-sections.

Castro, I.P. CFD for External Aerodynamics in the Built Environment. The QNET-CFD Network Newsletter - Vol. 2: No. 2 – July 2003, pp 4-7 (2003): The use of CFD to analyse exterior aerodynamics in the built environment is covered in this work. The article emphasises CFD's benefits over wind tunnel testing, notably its affordability and capacity to simulate intricate geometries. The limits of turbulence modelling and the necessity for precise boundary conditions are only two of the difficulties with employing CFD that are covered in the study.

Zhang et al. (2006) were experimental data and numerical simulations of particle transport and dispersion in ventilated rooms. The study used experimental and computational techniques to look into the movement and distribution of particles in ventilated spaces. The findings offered insightful information on how particles behave in ventilated interior spaces and demonstrated high agreement between experimental and numerical measures.

Yoshie et al. (2007) presented the findings of a collaborative effort for CFD prediction of pedestrian wind environment in J. Wind Eng. Ind. Aerodyn at the Architectural Institute of Japan. The objective of the study was to increase the precision of computational fluid dynamics (CFD) models of pedestrian wind settings. The findings demonstrated strong

agreement between the projected and observed values, suggesting that CFD has the capacity to predict pedestrian wind conditions with accuracy.

Van Hooff et al. (2014) Large eddy simulation (LES) and Reynolds-averaged Navier-Stokes (RANS) techniques were used to study counter-gradient diffusion in a slot-ventilated enclosure, and the results were reported in Computer Fluids. The goal of the study was to evaluate how well LES and RANS approaches predicted counter-gradient diffusion in an enclosure with slot ventilation. The findings demonstrated that while both LES and RANS approaches could predict counter-gradient diffusion, LES offered more precise predictions.

Van Hooff et al. (2013) Utilising the concentration decay approach, we assessed the natural ventilation of interior spaces. The study, which was published in Build. Environ., used CFD models to examine CO2 gas dispersion from a semi-enclosed stadium. The outcomes demonstrated that the stadium's ventilation performance could be predicted with accuracy using the concentration decay approach.

Van Hooff et al. (2012) published in J. Wind Eng. Ind. Aerodyn, full-scale assessments of indoor environmental conditions and natural ventilation in a sizable semi-enclosed stadium were performed. The study used full-scale measurements of the interior environmental conditions and natural ventilation in a sizable semi-enclosed stadium to examine the potential and limits of CFD validation.

Van Hooff et al. (2012) carried out particle image velocimetry (PIV) measurements and transitional flow analyses in a scaled-down ventilation system model. The research, which was published in Build. Environ., looked into transitional flow behaviour in ventilation systems using a free plane jet and the Coanda effect.

Van Hooff et al. (2010) CFD simulations, which were published in Comput. Fluids, looked at the impact of wind direction and urban surrounds on a big semi-enclosed stadium's natural ventilation. The study sought to determine how the stadium's natural ventilation performed in relation to wind direction and the surrounding urban environment.

Van Hooff et al. (2010) provided a case study of a high-resolution grid for modelling coupled urban wind flow and interior natural ventilation in Environ. Modelling

software. The goal of the study was to determine if CFD models could accurately forecast how a huge, semi-enclosed stadium would naturally ventilate under various wind conditions.

Tominaga et al. (2015) carried out wind tunnel tests on a generic building's cross-ventilation flow with pollutant dispersion under protected and uncovered settings, as reported in Build. A generic building's cross-ventilation flow and the behaviour of pollutants under various wind conditions were the subjects of the investigation.

Tominaga et al. (2010) The state-of-the-art in computational fluid dynamics (CFD) modelling approaches for near-field pollution dispersion in urban contexts is reviewed by Y. Tominaga and coworkers in this publication. The impacts of structures, topography, and other barriers are discussed in the authors' discussion of the difficulties involved in simulating pollution dispersion in the complex and varied urban environment. The study gives a thorough analysis of the many CFD models and methodologies, including Reynolds-averaged Navier-Stokes (RANS) models, large-eddy simulation (LES), and hybrid RANS-LES models, that have been created to predict pollution dispersion in metropolitan environments. The authors also go through the many turbulence models, such as the k- and k-models, that have been applied to CFD simulations of urban pollution dispersion.

Singh et al. (2015) An overview of CFD modelling of air flow and heat transfer in buildings, including applications for natural ventilation, thermal comfort, and energy efficiency, was given. They emphasised the need of using experimental data to calibrate and validate CFD models.

Natarajan and Perumal (2017) included themes including wind-driven ventilation, buoyancy-driven ventilation, and mixed-mode ventilation in a study of CFD analysis of natural ventilation in buildings. They also spoke about different simulation methods and difficulties in modelling complicated geometries.

Shanmuganathan and Velraj (2016) focuses on the implications of interior air quality, HVAC systems, and thermal comfort in the numerical modelling of indoor air flow and heat transfer in buildings. For trustworthy simulations, they emphasised the significance of precise boundary conditions and meshing.

Singh et al. (2016) presented a thorough study of CFD analysis of heat transport in buildings, covering a variety of applications including radiation, phase change, forced convection, and natural convection. They spoke about the benefits and drawbacks of various numerical techniques and models.

Dash et al. (2014) examines the impacts of various turbulence models, boundary conditions, and building layouts on interior air flow and heat transfer in buildings using CFD modelling. They also talked about how difficult it is to predict indoor air quality and thermal comfort.

CHAPTER 3

METHODOLOGY

In order to anticipate fluid flows, computational fluid dynamics (CFD) simulation has become widely used in engineering applications. It entails employing finite volume or finite element methods to quantitatively solve the governing equations of fluid motion. The turbulence model, numerical scheme, and boundary conditions are only a few of the variables that affect how accurate and reliable CFD simulations are. In CFD simulations, which include five steps—geometry, meshing, setup, solution, and result—ANSYS software is frequently utilised. The setup stage entails establishing the fluid parameters, boundary conditions, and numerical techniques to be utilised in the simulation. The geometry and meshing processes define the geometry and mesh, respectively. In the solution stage, the governing equations are resolved, and in the result step, the simulation results are examined and analysed. The (k-) turbulence model in ANSYS software is used in the current work to forecast the mean flow characteristics of turbulent flow conditions using CFD simulation methods.

Numerical model development for CFD simulation typically involves several steps to ensure the accuracy and reliability of the simulation results. Here are the detailed steps involved in numerical model development for CFD simulation:

3.1 PROBLEM DEFINITION

The first step in numerical model development is to define the problem. This involves determining the physical problem, the flow domain, and the boundary conditions. The problem definition should be based on the application and the desired objectives of the simulation. The problem is related to the simulation of airflow around a square-shaped building model with a dimension of 60 meters.

Predicting the flow characteristics and assessing how well the building reduces wind speed in the immediate vicinity are the goals. It is believed that the structure is situated in an open region with a constant wind speed. Computational Fluid Dynamics (CFD) methods will be used to run the simulation, and the (k-) turbulence model will be used to simulate turbulence. CAD software will be used to represent the building's shape, and a mesh

will be created to discretize the computational domain. Based on the demands of the situation, the boundary conditions and beginning conditions for the simulation will be chosen. In order to assess how the building would affect the surrounding airflow, including the flow separation, velocity profiles, and pressure distribution, the simulation results will be examined.

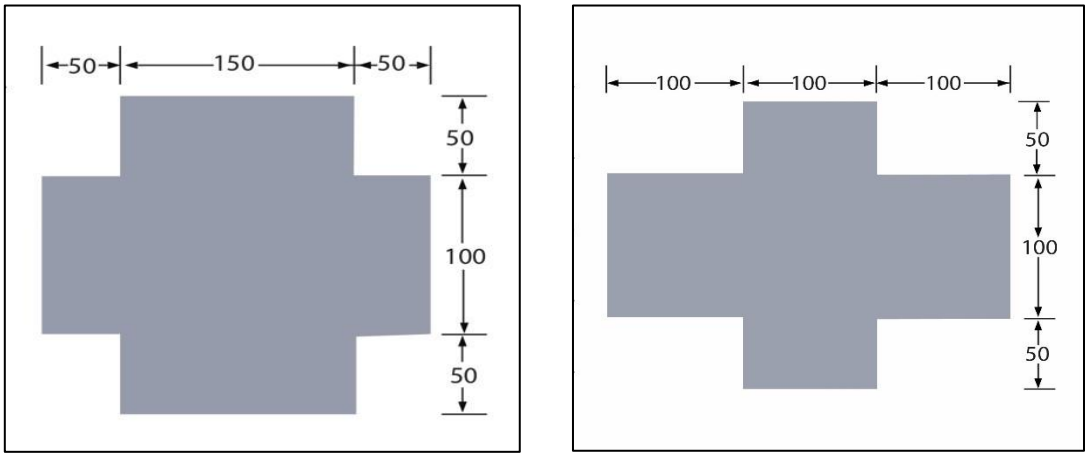

Figure 1: Plus shaped Model 1 and 2

3.2 GEOMETRY MODELLING

The second step involves creating the 3D model of the physical domain in which the fluid is to be analysed. This involves defining the shape, size, and location of the objects in the domain, such as walls, obstacles, and openings. Geometry modelling is a crucial step in computational fluid dynamics (CFD) simulations as it involves creating a 3D representation of the physical system being studied. The geometry modelling stage starts with collecting the relevant information about the system and creating a 3D model using specialized software tools such as ANSYS.

In the case of simulating a square-shaped building, the geometry modelling would involve creating a 3D model of the building in the software. This would require defining the dimensions and properties of the building such as its length, width, and height, and the location and size of doors, windows, and any other openings in the building. Geometry modelling is a crucial step in CFD simulations, as the accuracy of the model determines the accuracy of the simulation results. Therefore, it is important to spend time and effort in creating an accurate and realistic geometry model of the system being studied.

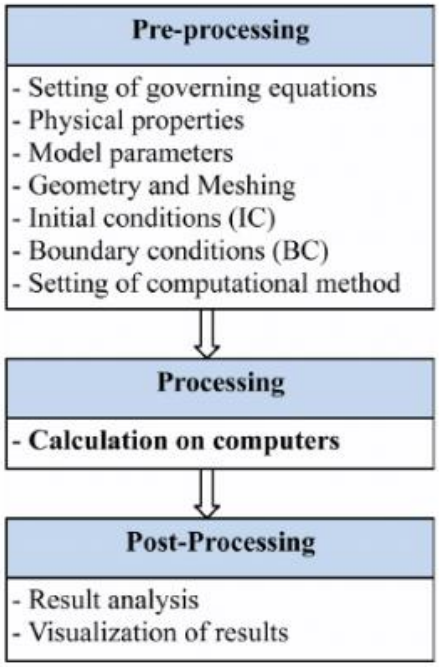

Figure 2: Computation procedure of CFD simulation

3.3 MESH GENERATION

After the geometry of the problem has been created, the domain needs to be divided into smaller elements or cells to generate a mesh. This process is called meshing and it is a crucial step in CFD simulation. The quality and density of the mesh have a significant impact on the accuracy and computational efficiency of the simulation. A mesh that is too coarse may not capture the details of the flow accurately, whereas a mesh that is too dense may result in longer simulation times and require more computational resources. Thus, it is important to strike a balance between the mesh density and computational efficiency. Various meshing techniques are available in CFD software, including structured, unstructured, and hybrid meshing, and the appropriate method is chosen based on the geometry and complexity of the problem.

Meshing of faces involves dividing the surfaces of the geometry into small planar elements or triangular facets. This is done by applying a surface meshing algorithm, which can be either automatic or manual. In automatic meshing, the software automatically creates a mesh based on the desired level of refinement, while in manual meshing, the user has more

control over the mesh quality and can adjust it according to the specific needs of the simulation.

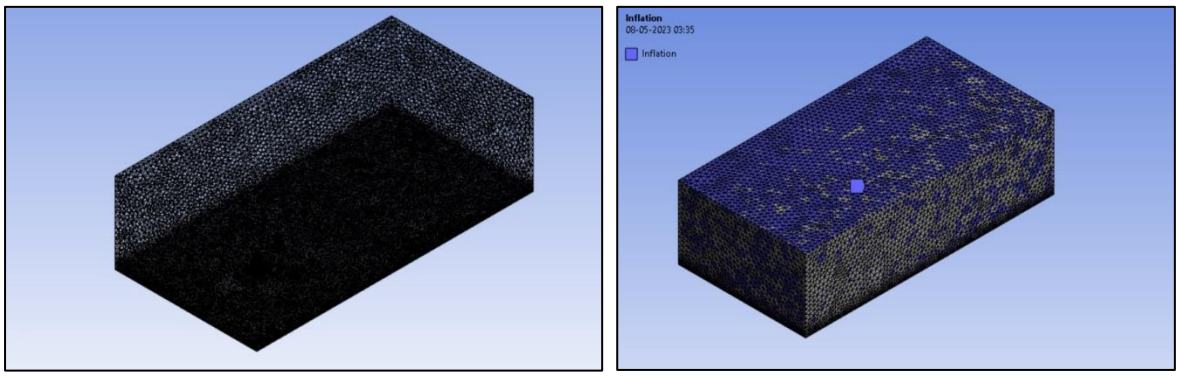

Figure 3: Meshing of Face and Inflation

Meshing of inflation is a process where additional layers of mesh are added near the walls to capture the near-wall flow physics accurately. The size of the inflation layer is typically chosen based on the distance from the wall, and it should be dense enough to capture the boundary layer but not too dense to affect the computational efficiency. Inflation layers help in better resolution of flow gradients near the wall and improve the accuracy of the CFD simulation.

3.4 NUMERICAL METHOD SELECTION

The next step is to select a numerical method for solving the governing equations of fluid flow. Common numerical methods used in CFD simulations include finite volume, finite element, and spectral methods. The next step is to select a suitable turbulence model and other physics models, such as heat transfer, multiphase flow, or chemical reactions, depending on the specific problem.

Scope	
Scoping Method	Geometry Selection
Geometry	13 Faces
Definition	
Suppressed	No
Type	Element Size
Element Size	8.e-003 m
Advanced	
Defeature Size	Default (1.e-003 m)
Influence Volume	No
Behavior	Soft
Growth Rate	Default (1.2)
Capture Curvature	No
Capture Proximity	No

Scope	
Scoping Method	Geometry Selection
Geometry	1 Face
Definition	
Suppressed	No
Type	Element Size
Element Size	8.e-002 m
Advanced	
Defeature Size	Default (1.e-003 m)
Influence Volume	No
Behavior	Soft
Growth Rate	Default (1.2)
Capture Curvature	No
Capture Proximity	No

Figure 4: Face sizing

Scope	
Scoping Method	Geometry Selection
Geometry	1 Body
Definition	
Suppressed	No
Boundary Scoping Method	Geometry Selection
Boundary	13 Faces
Inflation Option	Smooth Transition
Transition Ratio	Default (0.77)
Maximum Layers	6
Growth Rate	1.2
Inflation Algorithm	Pre

Figure 5: Inflation

Scope	
Scoping Method	Geometry Selection
Geometry	1 Body
Definition	
Suppressed	No
Method	Automatic
Element Order	Use Global Setting

Figure 6: Automatic Method

3.5 BOUNDARY CONDITIONS

Boundary conditions are an essential aspect of any CFD simulation. They specify the conditions at the boundaries of the computational domain, which the numerical solver uses to solve the governing equations of the fluid flow. In other words, boundary conditions define how the fluid interacts with the boundaries of the domain.

There are two types of boundary conditions:

1) Physical boundary conditions and
2) Mathematical boundary conditions.

Physical boundary conditions are based on the physics of the problem being simulated and describe the actual physical conditions at the boundary. Mathematical boundary conditions are used to ensure the numerical solution is well-posed and stable. Physical boundary conditions can be further divided into two types:

1) Velocity boundary conditions and
2) Pressure boundary conditions

Velocity boundary conditions prescribe the velocity of the fluid at the boundary. This is done by specifying either the velocity components (u, v, w) or the velocity magnitude and direction (u, v, w). Pressure boundary conditions specify the pressure at the boundary. These conditions can be either a fixed pressure value or a gradient of pressure between two points. It is essential to select the appropriate boundary conditions for each simulation, as these conditions have a significant impact on the accuracy and reliability of the results. Improper boundary conditions can lead to numerical instability or incorrect results, so careful attention must be paid to this step of the simulation process.

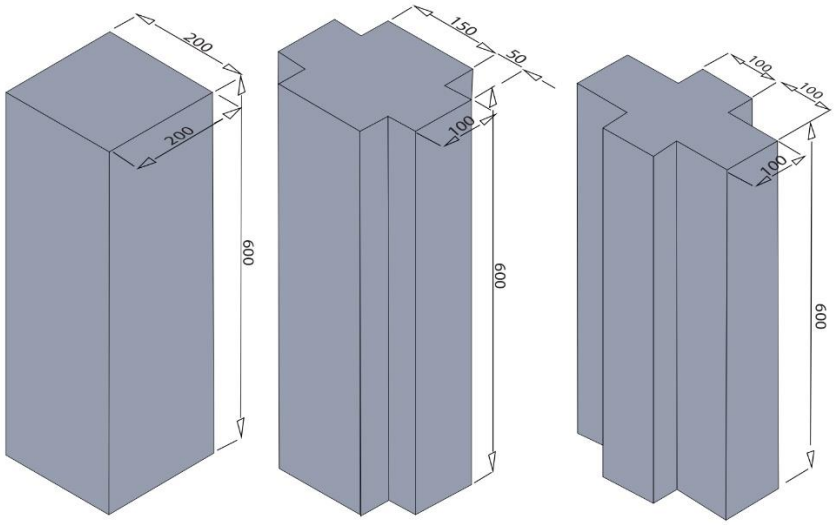

Figure 7: Square Model and Plus Shape Model 1 and 2

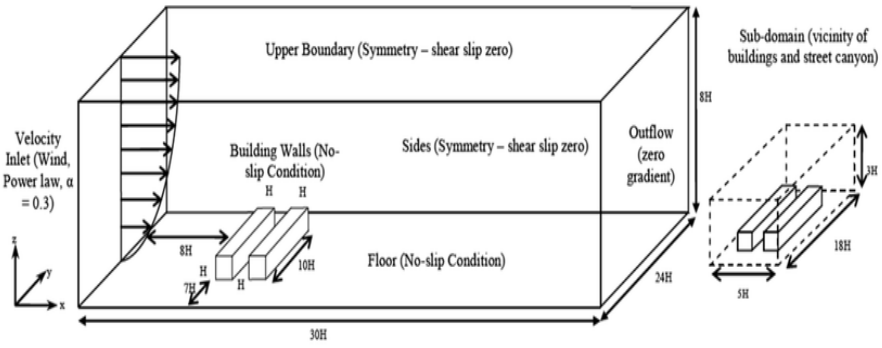

Figure 8: Alternate Domain size for larger boundary conditions

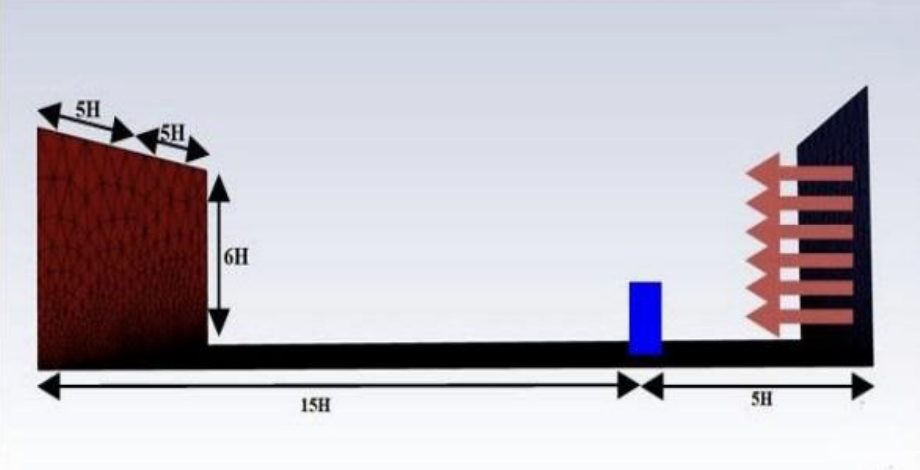

Figure 9: Computational domain and boundary conditions for the CFD simulation set up

3.6 SOLVER SELECTION

The next step is to select a solver that can solve the governing equations numerically. There are many commercial and open-source solvers available for CFD simulations, such as ANSYS Fluent. Selecting the appropriate solver in ANSYS Fluent is an essential step in CFD simulation as it can significantly impact the accuracy and speed of the solution. ANSYS Fluent provides a range of solver options that can handle different types of flows and physics, including steady-state and transient solvers, compressible and incompressible flows, multiphase flows, and turbulence models.

The steady-state solver is suitable for simulations with a steady flow field, while the transient solver is required for simulations with unsteady flows. Compressible flows, such as high-speed flows and gas dynamics, require the use of the compressible solver, which takes into account the changes in density due to pressure and temperature variations. Incompressible flows, such as low-speed flows and liquid flows, can be simulated using the incompressible solver, which assumes that the fluid density is constant.

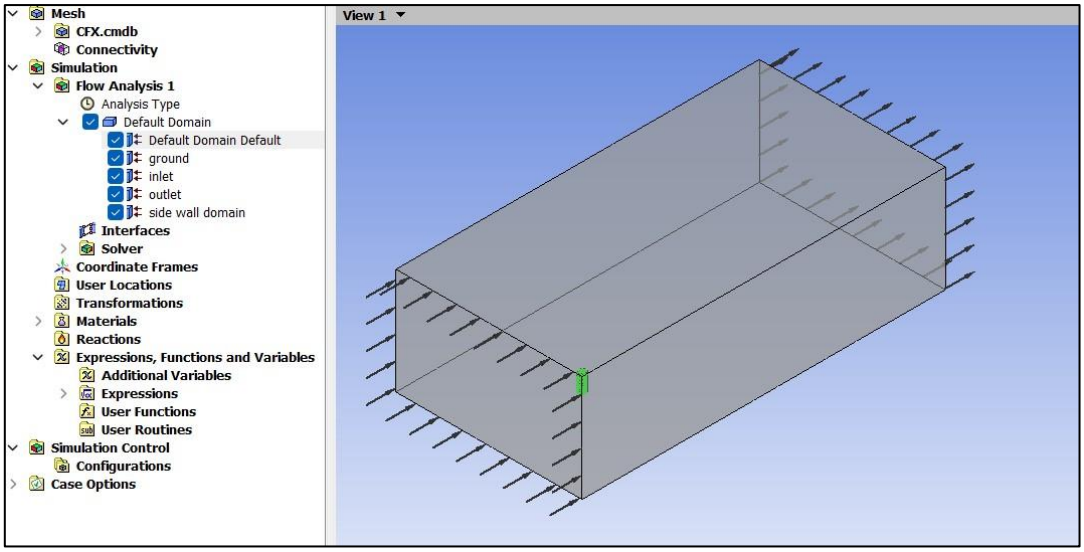

Figure 10: Default domain

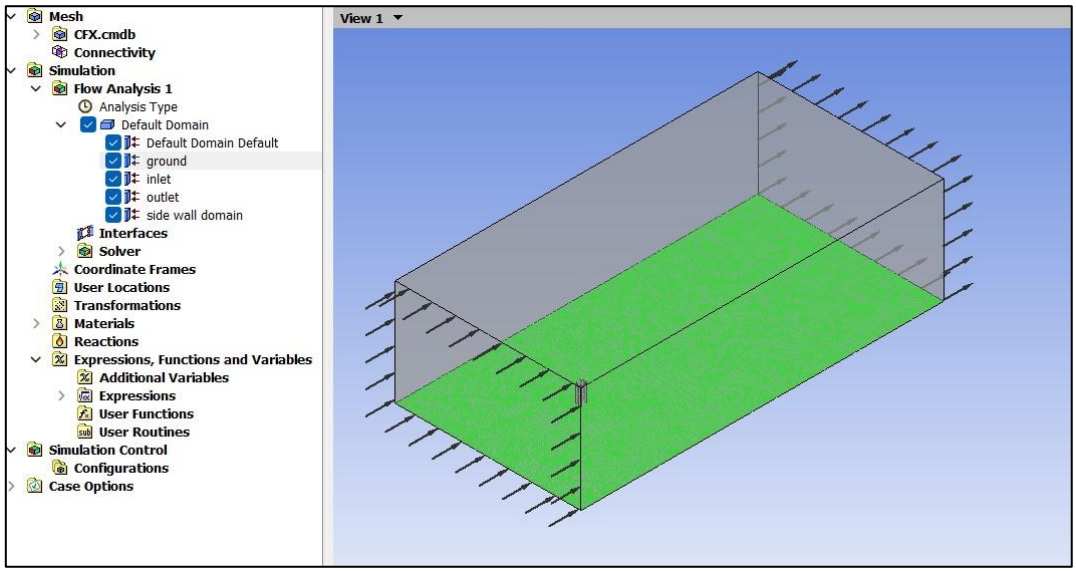

Figure 11: Ground

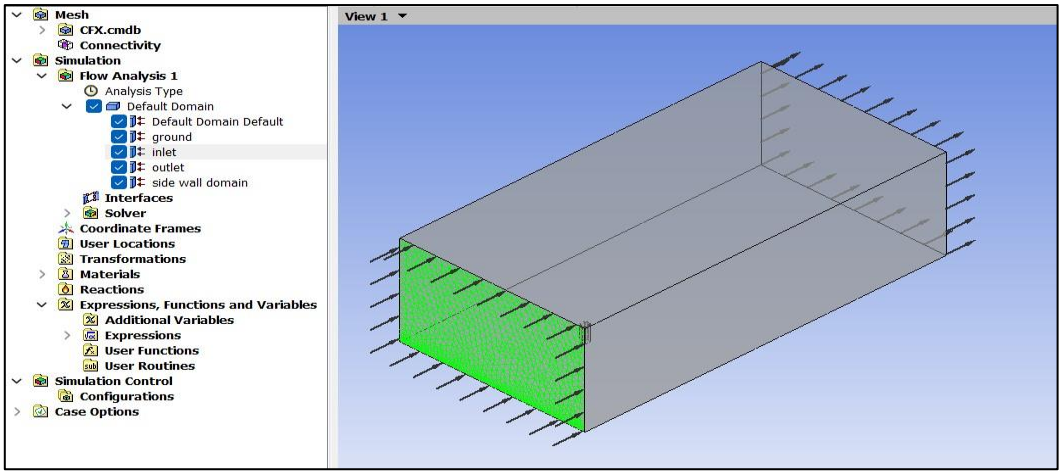

Figure 12: Inlet

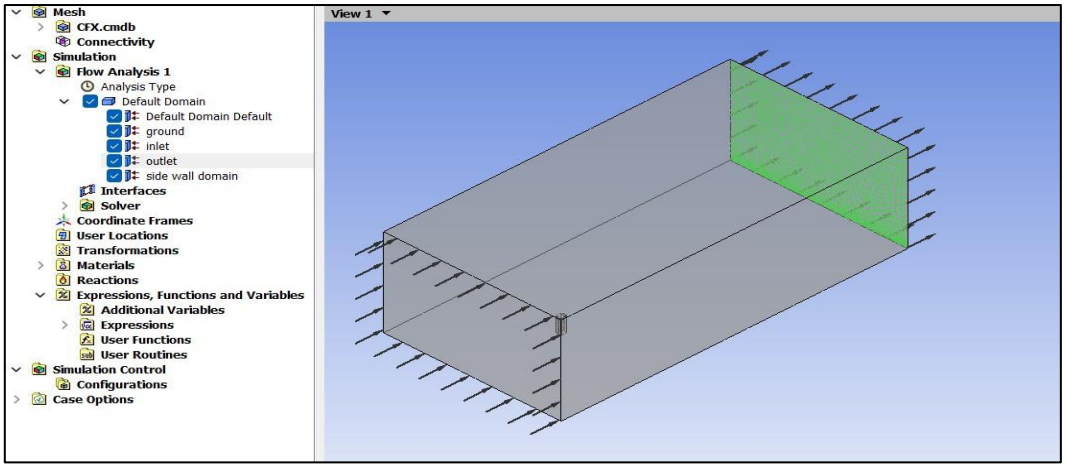

Figure 13: Outlet

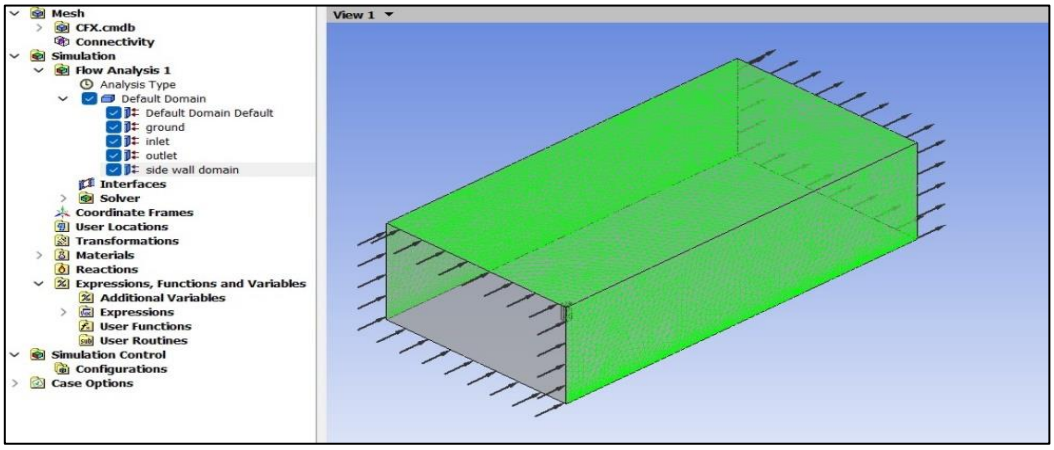

Figure 14: Side walls

3.7 SIMULATION SETUP

Once the solver has been selected, the next step is to set up the simulation. This involves specifying the numerical settings, such as the time step size, convergence criteria, and solver options.

Simulation setup is an important step in CFD simulation as it involves defining the numerical settings required to solve the governing equations. The following are the typical settings that need to be specified in the simulation setup:

- **Time step size:** The time step size is the amount of time taken by the solver to advance the solution from one time level to the next. It is an important parameter that affects the accuracy and stability of the solution. The time step size should be small enough to capture the transient behavior of the flow, but not too small to increase the computational cost.
- **Convergence criteria:** The convergence criteria are the thresholds that determine when the solution has converged. These criteria can be specified for different variables, such as the residual error, mass flow rate, or temperature. The convergence criteria should be tight enough to ensure a converged solution but not too tight to prevent the solution from converging.
- **Solver options**: The solver options refer to the various settings that can be used to control the solver's behavior. For example, the user can specify the turbulence model, the type of discretization scheme, and the type of pressure-velocity coupling. The solver options should be set appropriately to ensure an accurate and stable solution.
- **Boundary conditions:** The flow variables' values at the domain's boundaries are determined by the boundary conditions. They consist of the wall conditions, symmetry conditions, and inlet and outflow conditions. The physical issue being simulated should be used to determine the boundary conditions.
- **Initial conditions:** The initial conditions are the values of the flow variables at the beginning of the simulation. They can be set to zero or based on experimental data or previous simulations.
- **Solution control:** The solution control settings allow the user to control the output of the simulation. For example, the user can specify the frequency of the solution output or the type of variables to be saved.

3.8 SOLUTION PROCEDURE

The solution procedure is a crucial step in the CFD simulation process, as it involves solving the governing equations numerically using the selected solver and numerical method. This step typically involves several iterations, and the convergence of the solution should be monitored closely to ensure accurate results. During the solution procedure, the solver applies the selected numerical method to solve the governing equations of fluid motion.

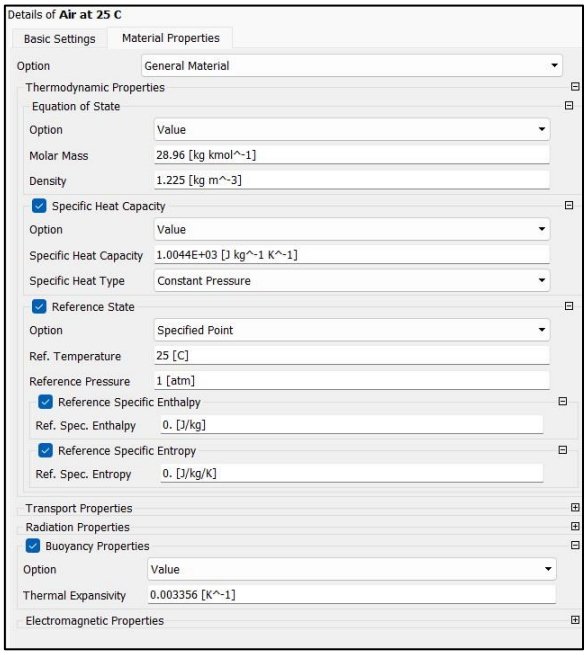

Figure 15: Material Properties

The numerical method discretizes the domain into small elements or cells and applies numerical algorithms to solve the equations at each cell. The solution process typically involves solving for the velocity and pressure fields in the domain. The convergence of the solution is monitored by comparing the residual values of the governing equations between successive iterations. The residual values represent the difference between the values of the governing equations calculated at each iteration and the actual values of the equations. As the solution converges, the residual values should decrease until they reach a specified

tolerance level. If the residual values do not decrease or the solution diverges, the solver settings may need to be adjusted or the mesh may need to be refined.

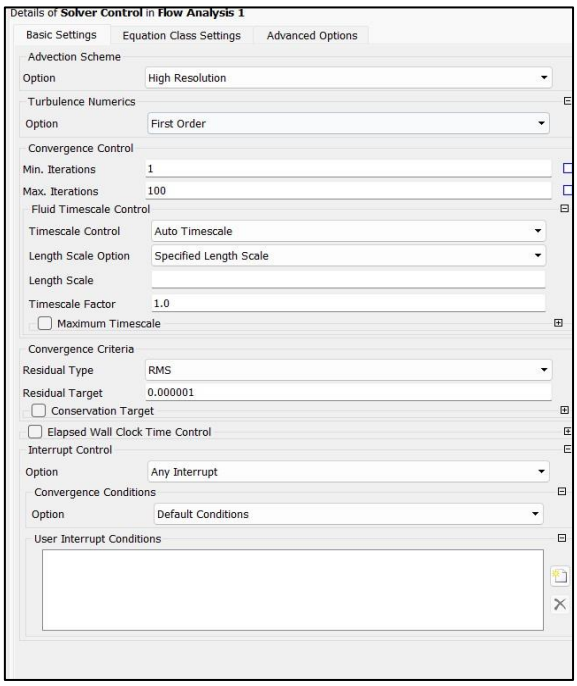

Figure 16: Solver Control

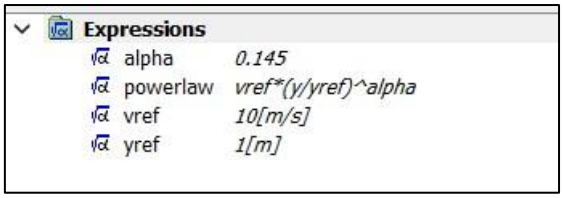

Figure 17: Expression

To ensure accurate results, it is important to choose appropriate solver settings and numerical methods that are appropriate for the specific problem being solved. In addition, the solution procedure should be performed on a computer with sufficient computational power to handle the calculations involved in the simulation.

3.9 POST-PROCESSING

Finally, the simulation results are analysed and interpreted using post-processing techniques. This involves visualising the results, such as velocity, pressure, and temperature distributions, and extracting relevant data, such as flow rates and heat transfer coefficients.

In summary, numerical model development for CFD simulation involves several steps, including problem definition, geometry modelling, mesh generation, physics modelling, numerical method selection, boundary conditions, solver selection, simulation setup, solution procedure, and post-processing. These steps must be carefully followed to ensure accurate and reliable simulation results.

CHAPTER 4

NUMERICAL SIMULATION OF MODEL 1

The aim of this study was to conduct a CFD simulation of the flow field over a square-shaped building model of 60 meters. The simulation was performed to gain insights into the flow characteristics, such as pressure contours, vertical and horizontal streamlines, and pressure coefficients at various angles ranging from 0 to 180 degrees with an interval of 30 degrees. To achieve this, we developed a numerical model using ANSYS Fluent software. The model included the geometry of the square-shaped building and was meshed using a structured meshing technique to generate a high-quality mesh. After the mesh was generated, we applied boundary conditions, including inlet and outlet velocities, wall boundary conditions, and turbulence parameters, to the model.

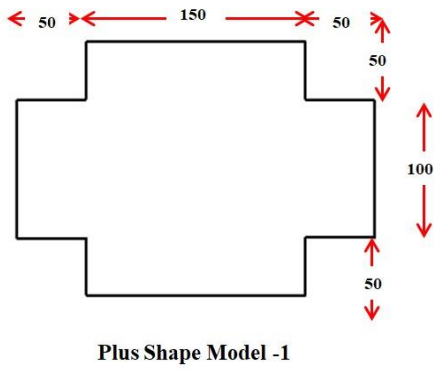

Figure 18: Geometry of Model 1

The solver used in this study was the pressure-based solver in ANSYS Fluent, which was chosen for its ability to accurately capture complex flows. The simulation was run for a specified time, and the convergence of the solution was monitored at each iteration. Once the simulation was complete, the results were analysed to gain insights into the flow characteristics. The pressure contours provided information about the pressure distribution over the surface of the building, while the vertical and horizontal streamlines gave a

visualization of the flow patterns. Additionally, the pressure coefficients at various angles provided a better understanding of the aerodynamic performance of the building.

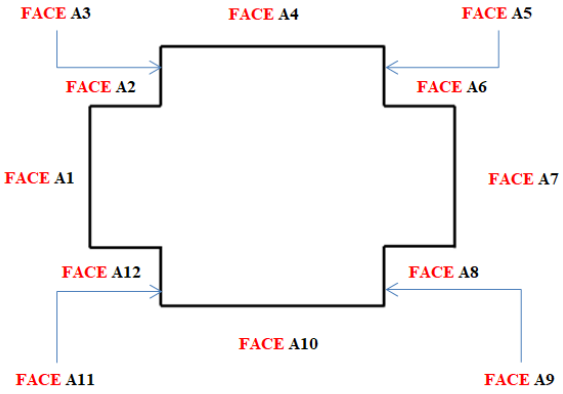

Figure 19: Naming of Faces

Overall, the CFD simulation of the flow field over the square-shaped building model provided valuable insights into the flow characteristics and aerodynamic performance. These insights can be used to optimize the design of buildings and reduce energy consumption in the built environment.

4.1 PRESSURE COEFFICIENT

The pressure coefficient (Cp), which is a dimensionless number in fluid dynamics, gives details on the local pressure distribution on a body's surface. It is determined by dividing the dynamic pressure by the difference between the local pressure and the free-stream pressure. Given that the fluid density is and the free-stream velocity is V, the dynamic pressure is given by the formula 1/2 * * V2. The pressure coefficient in CFD simulations may be computed using the simulation output.

In aerodynamic research, the pressure coefficient is frequently employed to examine the pressure distribution along the surface of an airfoil or wing. It is used in building aerodynamics to analysis the pressure distribution on a building's surface and can offer information about the wind stresses on the structure. The drag and lift forces on a body may be calculated using the pressure coefficient and are significant in many engineering applications. Using the results of the CFD simulation, we computed the pressure coefficients

at various angles on the surface of the square-shaped building model in this study. These pressure coefficients provide important information about the building's wind loads and the local pressure distribution.

4.2 PRESSURE CONTOURS

In ANSYS' CFX mode, pressure contours are obtained after analysis. Pressure contours are used to show how the pressure values on a surface vary over time. The pressure contours below demonstrate the relative difference in pressure effect at wind inclination ranging from 0 to 180 degrees at a 30degree interval. The pressure contours obtained lead to the following deductions:

1. **When wind angle is 0°**

The range of average pressure values for the wind inclination angle of 0^0 is between **[-23.88, 31.99].** The maximum positive and negative pressure values of 31.99 and -23.88, respectively, occur on Face A1 and A11. The range of pressure coefficient Cp lies in the range ε **[-0.39, 0.52]**. The maximum positive and negative values of 0.52 and -0.39 occur on Face A1 and A11, indicating the areas of the building that will experience the highest wind load.

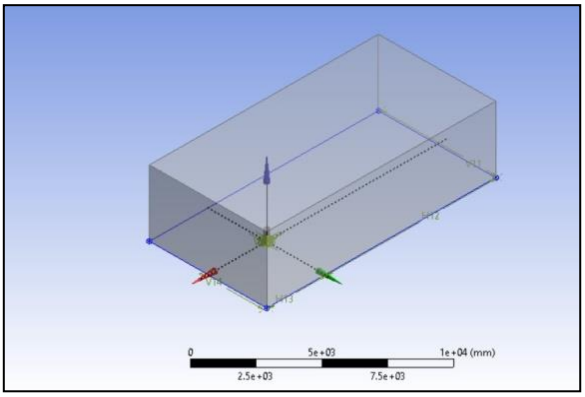

Wind Angle 0 degree				
Faces	Range of pressure	Average pressure	Range of Cp	Average Cp
A1	(-37.20,49.58)	31.99	(-0.61,0.81)	0.52
A2	(-45.23,15.45)	5.77	(-0.74,0.25)	0.09
A3	(-40.83,39.93)	9.22	(-0.67,0.65)	0.15
A4	(-54.79,-1.87)	-22.08	(-0.89,-0.03)	-0.36
A5	(-49.60,15.35)	6.18	(-0.81,0.25)	0.10
A6	(-28.85,-5.27)	-18.89	(-0.47,-0.09)	-0.31
A7	(-49.33,39.26)	9.85	(-0.81,0.64)	0.16
A8	(-27.66,-8.09)	-19.74	(-0.45,-0.13)	-0.32
A9	(-51.24,-0.41)	-21.15	(-0.84,-0.01)	-0.35
A10	(-26.97,-13.65)	-22.38	(-0.44,-0.22)	-0.37
A11	(-27.48,-19.04)	-23.88	(-0.45,-0.31)	-0.39
A12	(-26.51,-2.02)	-18.07	(-0.43,-0.03)	-0.29

Figure 20: Geometry and Pressure and Cp values

Table 1: Pressure contour of faces at 0-degree wind inclination

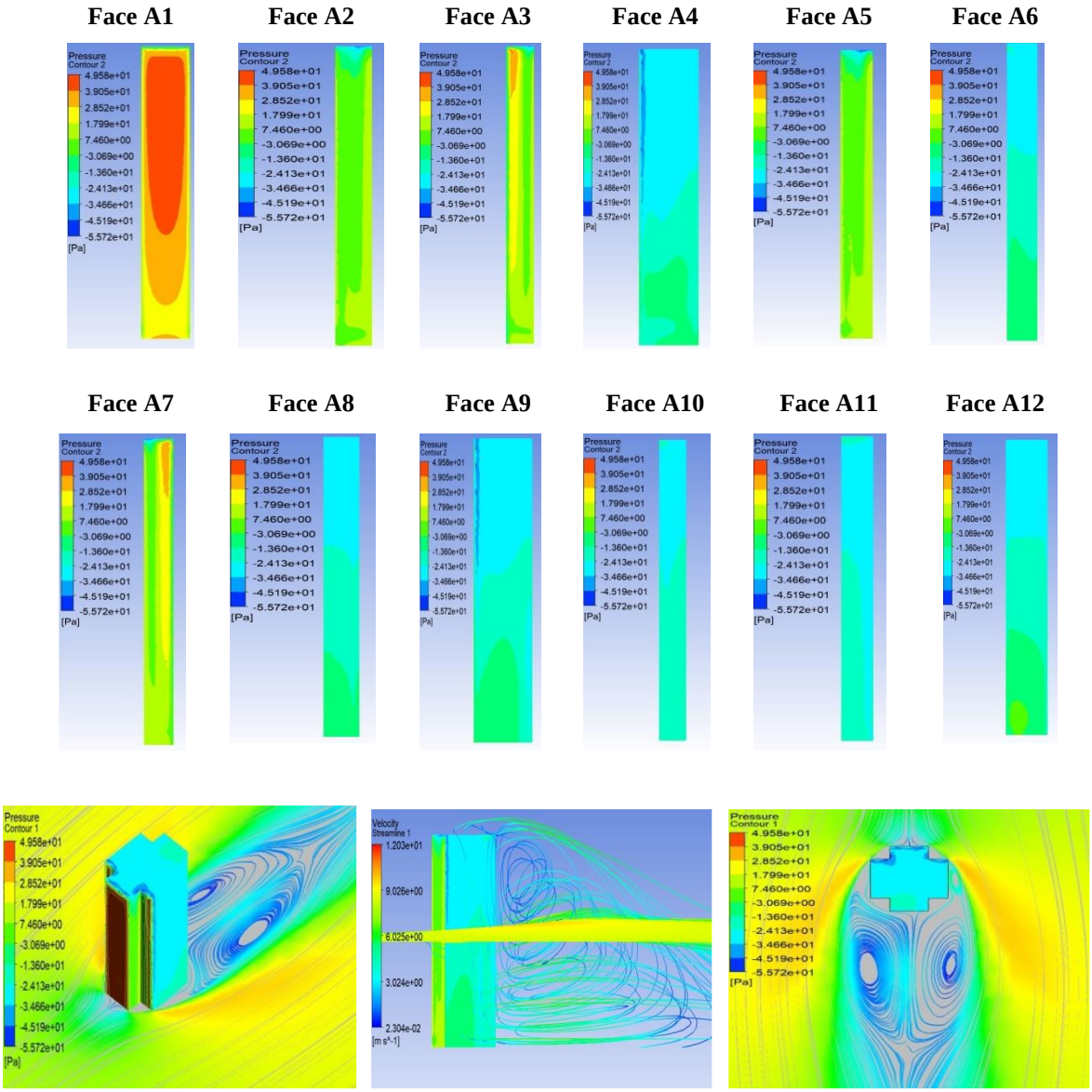

Figure 21: Horizontal and Vertical Streamlines for 0 degree wind inclination

Velocity streamlines are an important aspect of fluid flow visualization in CFD simulations. Streamlines are a graphical representation of the velocity vector field in a fluid flow, and they provide information about the flow patterns and directions. In CFD simulations, streamlines are typically calculated by solving the equations of motion for a large number of particles or fluid elements, and then plotting the paths of these elements over time. The resulting lines represent the direction of the fluid velocity at each point in the flow.

2. When wind angle is 30°

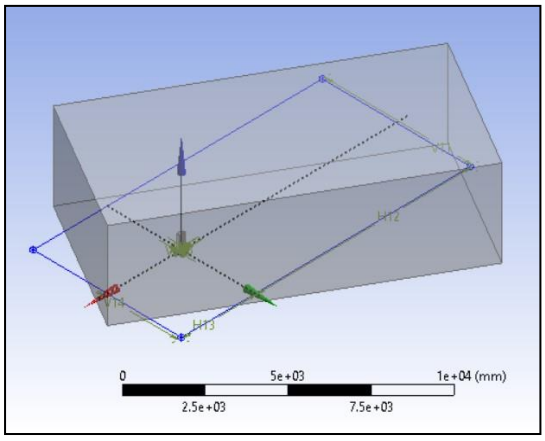

Wind Angle 30 degree				
Faces	Range of pressure	Average pressure	Range of Cp	Average Cp
A1	(-59.85, 48.76)	16.77	(-0.98,0.8)	0.27
A2	(-53.63,48.76)	37.85	(-0.36,0.6)	0.62
A3	(-56.67,48.81)	32.12	(-0.92,0.8)	0.52
A4	(-55.23,9.99)	(-9.33)	(-0.9,0.16)	-0.15
A5	(-59.85,-17.05)	(-30.62)	(-0.98, -0.28)	-0.63
A6	(-48.69,-12.36)	(-24.29)	(-0.79,-0.2)	-0.40
A7	(-50.37, -8.74)	(-31.50)	(-0.82,-0.14)	-0.51
A8	(-25.71,-12.52)	(-21.58)	(-0.42,-0.2)	-0.35
A9	(-43.26,-8.74)	(-20.49)	(-0.71,-0.14)	-0.33
A10	(-32.09,-6.71)	(-17.70)	(-0.52,-0.11)	-0.29
A11	(-27.41,-7.64)	(-17.43)	(-0.45,-0.12)	-0.28
A12	(-31.35,-8.87)	(-19.06)	(-0.51,-0.14)	-0.31

Figure 22: Geometry and Pressure and Cp values

Table 2: Pressure contour of faces at 30-degree wind inclination

Face A1	Face A2	Face A3	Face A4	Face A5	Face A6
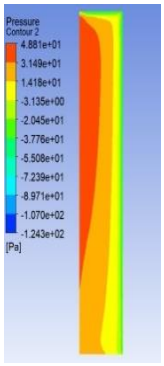	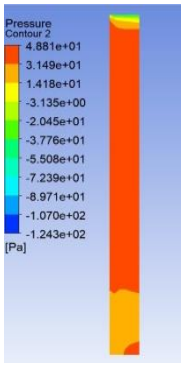	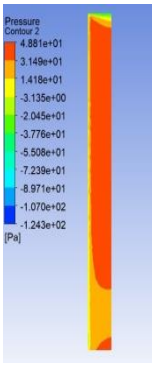	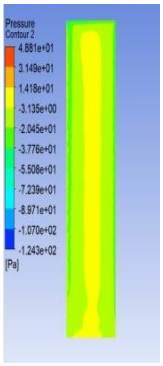	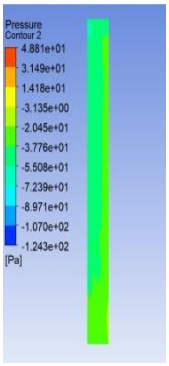	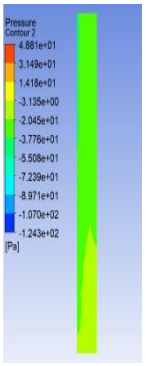

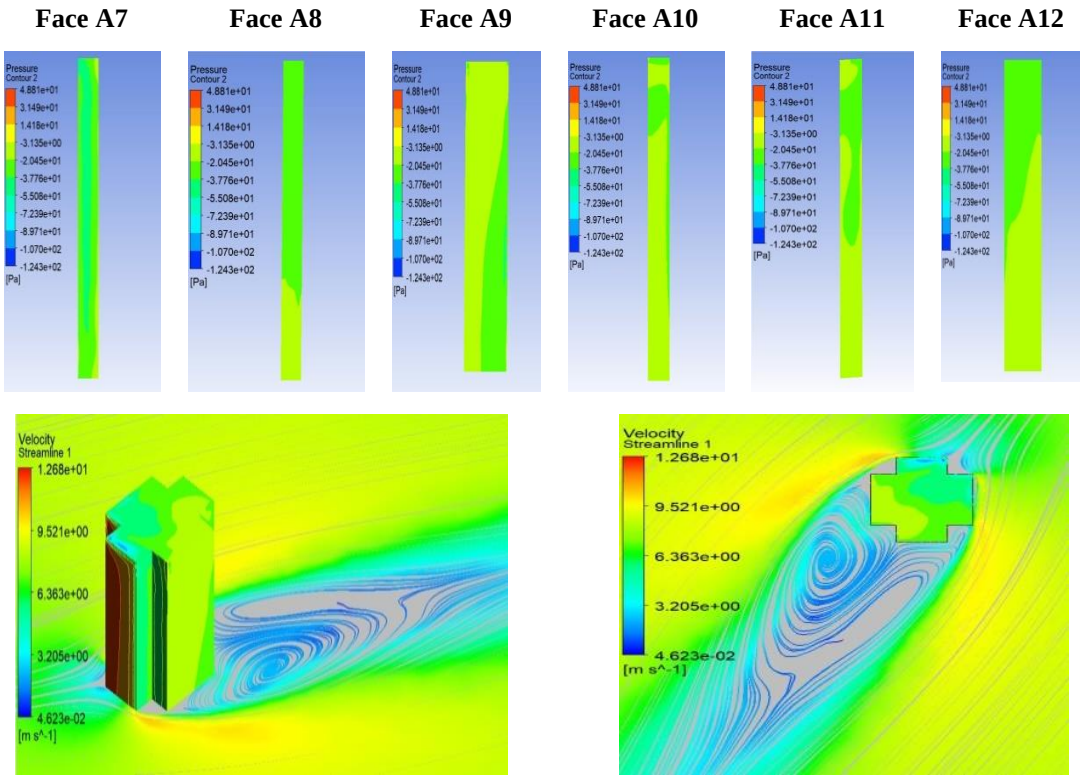

Figure 23: Horizontal and Vertical Streamlines for 30 degree wind inclination

The range of average pressure values for the wind inclination angle of 30^0 is between [-31.50, 37.85]. The maximum positive and negative pressure values of 37.85 and -31.50, respectively, occur on Face A2 and A7. The range of pressure coefficient Cp lies in the range ε [-0.63, 0.62]. The maximum positive and negative values of 0.62 and -0.63 occur on Face A2 and A5.

3. When wind angle is 60°

Table 3: Pressure contour of faces at 60-degree wind inclination

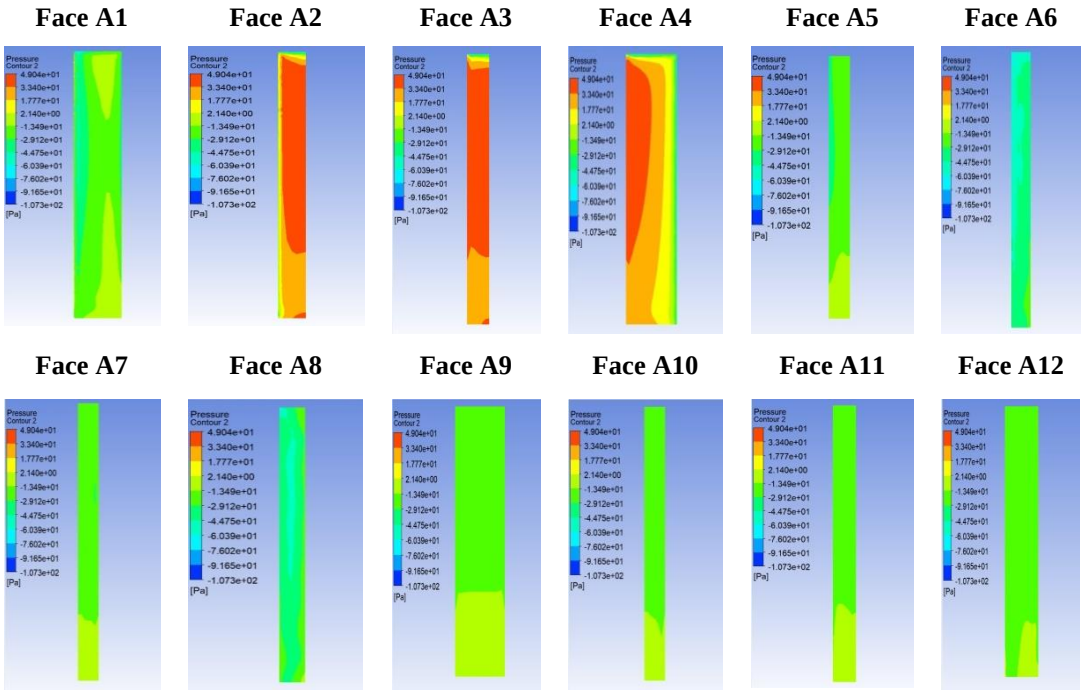

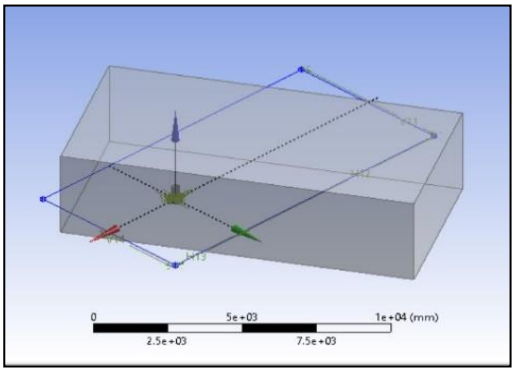

Wind Angle 60 degree				
Faces	Range of pressure	Average pressure	Range of Cp	Average Cp
A1	(-72.13,4.85)	-20.55	(-1.18,0.08)	-0.34
A2	(-71.76,47.86)	29.17	(-1.17,0.78)	0.48
A3	(-81.36,47.78)	35.95	(-1.33,0.78)	0.59
A4	(-70.89,49.04)	19.66	(-1.16,0.80)	0.32
A5	(-39.52,-6.73)	-21.08	(-0.65,-0.11)	-0.34
A6	(-65.02,-18.78)	-41.21	(1.06,-0.31)	-0.67
A7	(-29.84,-7.33)	-19.21	(-0.49,-0.12)	-0.31
A8	(-52.66,-11.02)	-35.03	(-0.86,-0.16)	-0.57
A9	(-27.28,-5.94)	-16.74	(-0.45,-0.10)	-0.27
A10	(-23.42,-8.81)	-17.86	(-0.38,-0.14)	-0.29
A11	(-23.75,-7.71)	-17.57	(-0.39,-0.13)	-0.29
A12	(-27.07,-10.30)	-19.37	(-0.44,-0.17)	-0.32

Figure 24: Geometry and Pressure and Cp values

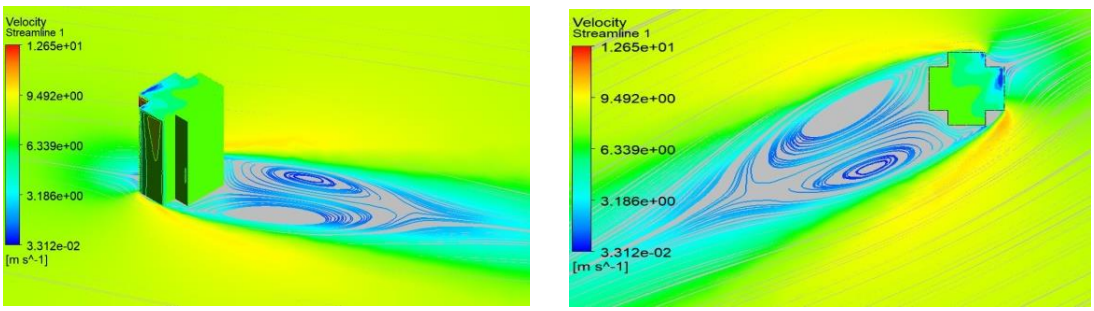

Figure 25: Horizontal and Vertical Streamlines for 60 degree wind inclination

The range of average pressure values for the wind inclination angle of 60^0 is between **[**-41.21, 35.95]. The maximum positive and negative pressure values of 35.95 and -41.21, respectively, occur on Face A3 and A6. The range of pressure coefficient Cp lies in the range ε [-0.67, 0.59]. The maximum positive and negative values of 0.59 and -0.67 occur on Face A3 and A6, indicating the areas of the building that will experience the highest wind load.

4. When wind angle is 90°

The range of average pressure values for the wind inclination angle of 90^0 is between **[**-25.75, 31.63]. The maximum positive and negative pressure values of 31.63 and -25.75, respectively, occur on Face A4 and A1. The range of pressure coefficient Cp lies in the range ε [-0.42, 0.52]. The maximum positive and negative values of 0.52 and -0.42 occur on Face A4 and A1, indicating the areas of the building that will experience the highest wind load.

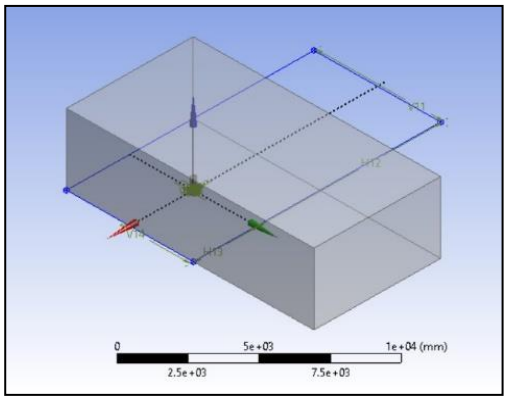

Wind Angle 90 degree				
Faces	Range of pressure	Average pressure	Range of Cp	Average Cp
A1	(-51.99,-4.56)	-25.75	(-0.85,-0.07)	-0.42
A2	(-38.30,38.3)	1.46	(-0.63,0.63)	0.02
A3	(-38.7,9.61)	-3.64	(-0.63,0.16)	-0.06
A4	(-39.1,49.1)	31.63	(-0.64,0.8)	0.52
A5	(-26.9,-16.8)	-23.70	(-0.44,-0.27)	-0.39
A6	(-40.6,10.7)	-1.13	(-0.66,0.17)	-0.02
A7	(-31.6,-16.8)	-24.55	(-0.52,-0.27)	-0.40
A8	(-38.4,38.7)	3.75	(-0.63,0.63)	-0.02
A9	(-31.9,-8.8)	-20.02	(-0.52,0.63)	-0.40
A10	(-28.8,-10.20)	-19.86	(-0.46,-0.17)	0.06
A11	(-29.2,-9.02)	-19.42	(-0.47,-0.15)	-0.32
A12	(-49.8,-6.23)	-22.07	(-0.81,-0.1)	-0.36

Figure 26: Geometry and Pressure and Cp values

Table 4: Pressure contour of faces at 30-degree wind inclination

Face A1	Face A2	Face A3	Face A4	Face A5	Face A6
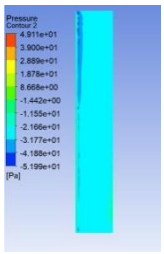	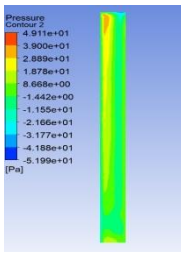	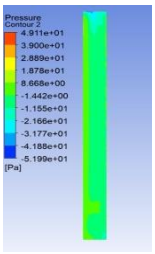	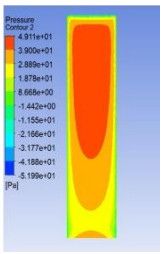	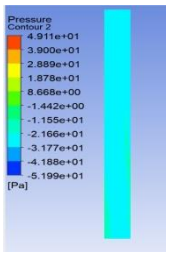	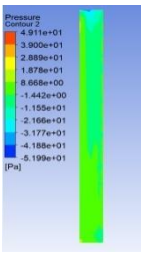

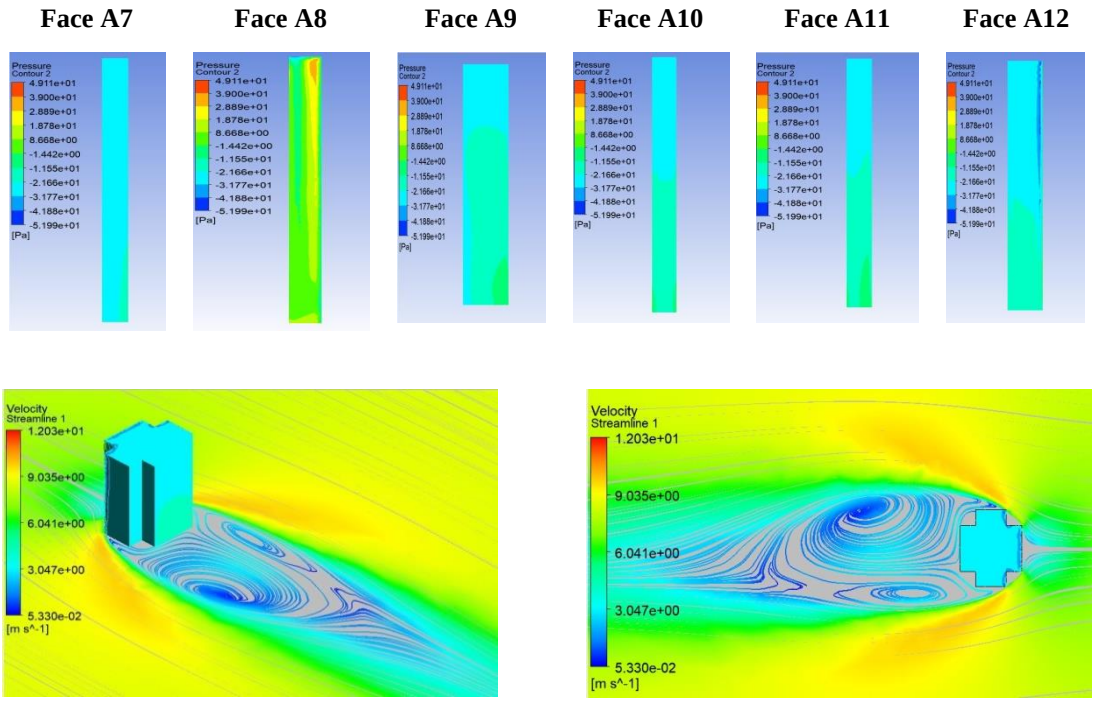

Figure 27: Horizontal and Vertical Streamlines for 0 degree wind inclination

5. When wind angle is 120°

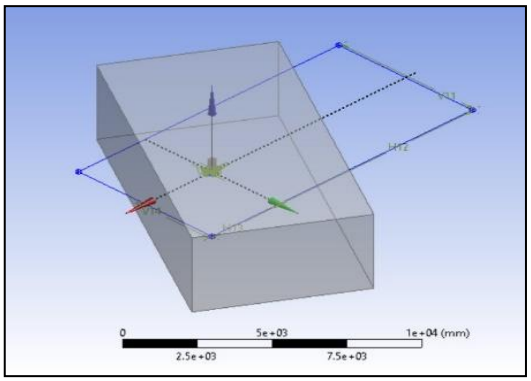

Wind Angle 120 degree				
Faces	Range of pressure	Average pressure	Range of Cp	Average Cp
A1	(-27.29,-10.99)	-19.46	(-0.45,-0.18)	-0.32
A2	(-51.8,-11.9)	-35.39	(-0.85,-0.19)	-0.58
A3	(-66.2,-19.7)	-41.58	(-1.08,-0.32)	-0.68
A4	(-74.2,49.3)	19.54	(-1.21,0.8)	0.32
A5	(-23.6,-8.2)	-17.39	(-0.39,-0.13)	-0.28
A6	(-67.2,48.1)	36.11	(-1.10,0.8)	0.59
A7	(-23.4,-8.93)	-17.79	(-0.38,-0.15)	-0.29
A8	(-74.8,48)	29.32	(-1.22,0.78)	0.48
A9	(-27.5,-6.48)	-16.72	(-0.45,-0.11)	-0.27
A10	(-29.9,-7.34)	-19.51	(-0.49,-0.12)	-0.32
A11	(-39.8,-7.15)	-21.47	(-0.65,-0.12)	-0.35
A12	(-71.2,1.98)	-20.47	(-1.16,0.03)	-0.33

Figure 28: Geometry and Pressure and Cp values

The range of average pressure values for the wind inclination angle of 120^0 is between [-41.58, 36.11]. The maximum positive and negative pressure values of 36.11 and -41.58, respectively, occur on Face A6 and A3. The range of pressure coefficient Cp lies in the range ε [-0.68, 0.59]. The maximum positive and negative values of 0.59 and -0.68 occur on Face A6 and A3, indicating the areas of the building that will experience the highest wind load.

Table 5: Pressure contour of faces at 120-degree wind inclination

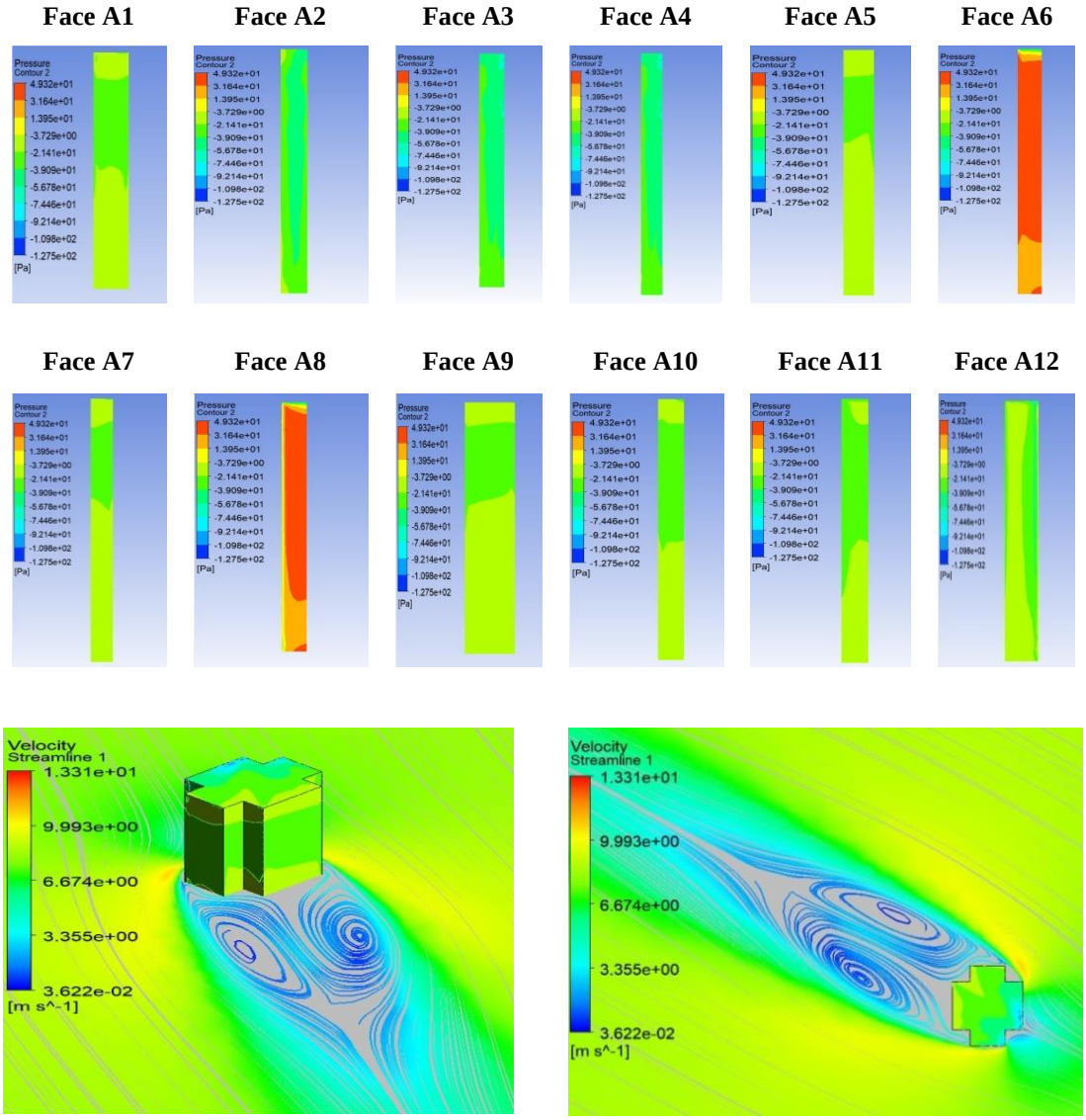

Figure 29: Horizontal and Vertical Streamlines for 0 degree wind inclination

6. When wind angle is 150°

The range of average pressure values for the wind inclination angle of 150^0 is between [-44.02, 38.03]. The maximum positive and negative pressure values of 38.03 and -44.02, respectively, occur on Face A8 and A11. The range of pressure coefficient Cp lies in the range ε [-0.80, 0.62]. The maximum positive and negative values of 0.62 and -0.80 occur on Face A8 and A5.

Table 6: Pressure contour of faces at 150-degree wind inclination

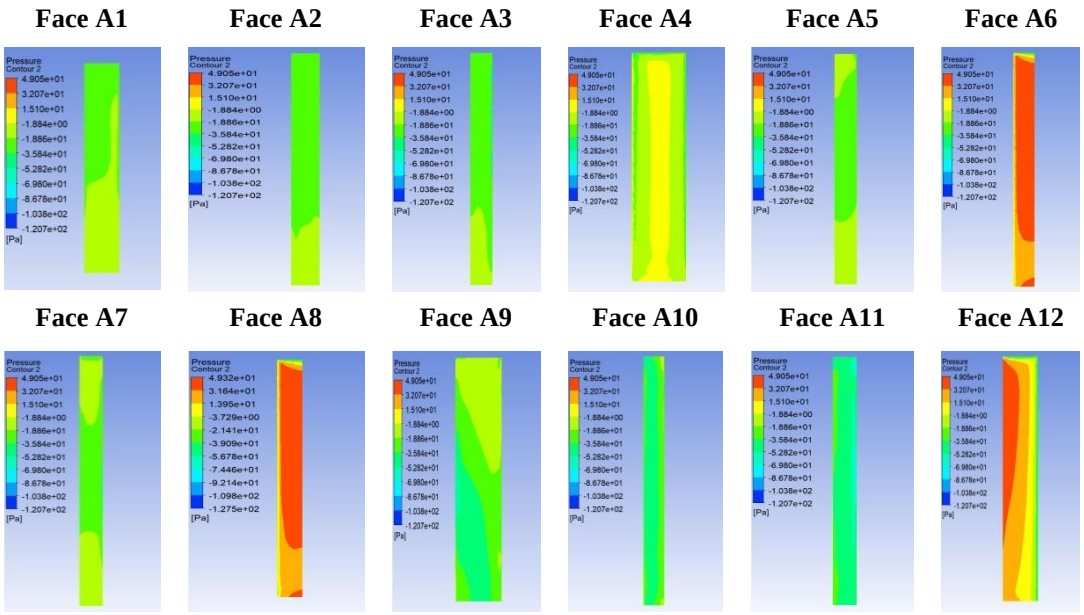

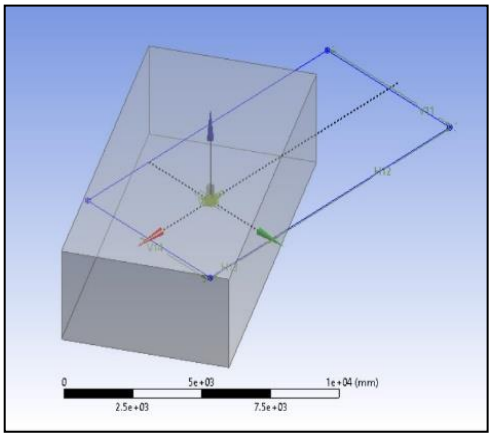

Wind Angle 150 degree				
Faces	Range of pressure	Average pressure	Range of Cp	Average Cp
A1	(-27.49,-10.22)	-17.87	(-0.45,-0.17)	-0.29
A2	(-24.3,-12.1)	-20.28	(-0.4,-0.2)	-0.33
A3	(-47.1,-11.9)	-22.80	(-0.77,-0.19)	-0.37
A4	(-52.1,17.2)	-7.85	(-0.85,0.25)	-0.13
A5	(-25.5,-8.01)	-18.44	(-0.42,-0.13)	-0.80
A6	(-56.9,49.1)	32.76	(-0.93,0.8)	0.53
A7	(-43.3,-7.93)	-19.73	(-0.71,-0.13)	-0.32
A8	(-53.6,48.9)	38.03	(-0.88,-0.8)	0.62
A9	(-61.2,-13.3)	-28.54	(-1,-0.22)	-0.47
A10	(-53.9,-10.5)	-35.97	(-0.88,-0.17)	-0.59
A11	(-69.8,-27.4)	-44.02	(-1.13,-0.45)	-0.72
A12	(-69.8,48.9)	14.97	(-1.13,0.8)	0.24

Figure 30: Geometry and Pressure and Cp values

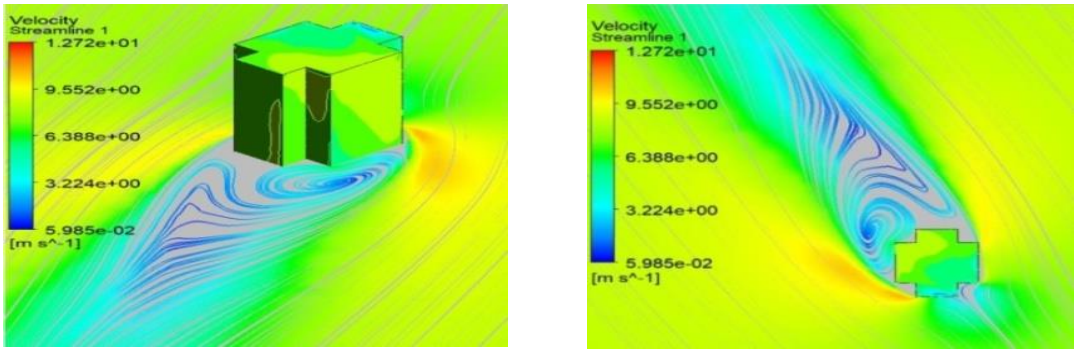

Figure 31: Horizontal and Vertical Streamlines for 0 degree wind inclination

7. When wind angle is 180°

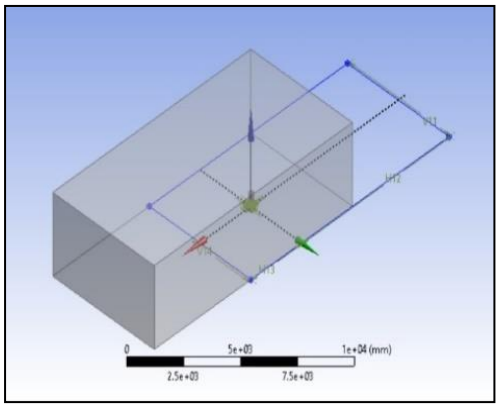

Wind Angle 180 degree				
Faces	Range of pressure	Average pressure	Range of Cp	Average Cp
A1	(-26.3,-2.3)	-18.05	(-0.43,-0.04)	-0.29
A2	(-25.7,-8.74)	-20.75	(-0.42,-0.14)	-0.34
A3	(-27.1,-5.16)	-19.68	(-0.44,-0.08)	-0.32
A4	(-51.8,0.02)	-23.64	(-0.85,0)	-0.39
A5	(-27.9,-10.7)	-22.15	(-0.46,0.17)	-0.36
A6	(-39.6,39.9)	8.85	(-0.65,0.65)	0.14
A7	(-29.6,-6.06)	-20.83	(-0.48,0.1)	-0.84
A8	(-44.1,16.5)	5.34	(-0.72,0.27)	0.09
A9	(-49,1.25)	-20.93	(-0.8,0.02)	-0.34
A10	(-43.9,40.6)	10.11	(-0.72,0.66)	0.17
A11	(-46.5,16.6)	6.49	(-0.76,0.27)	0.11
A12	(-34.5,49.8)	32.32	(-0.56,0.81)	0.53

Figure 32: Geometry and Pressure and Cp values

The range of average pressure values for the wind inclination angle of 180^0 is between [-23.64, 32.32]. The maximum positive and negative pressure values of 32.32 and -23.64, respectively, occur on Face A12 and A4. The range of pressure coefficient Cp lies in the range ε [-0.84, 0.53]. The maximum positive and negative values of 0.53 and -0.84 occur on Face A12 and A7.

Table 7: Pressure contour of faces at 180-degree wind inclination

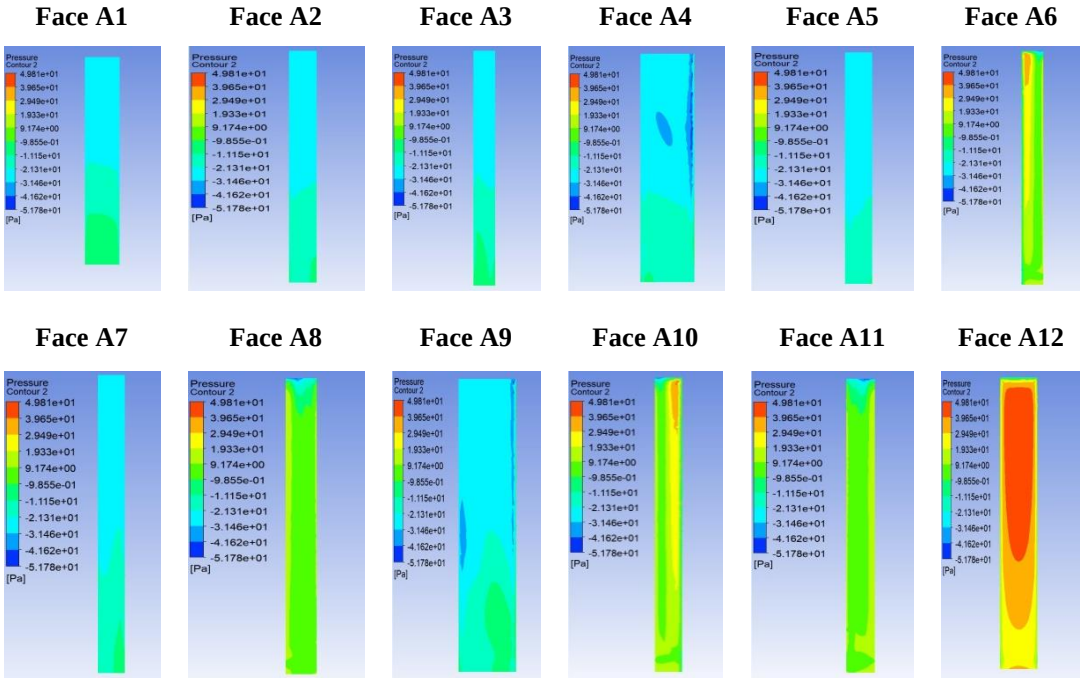

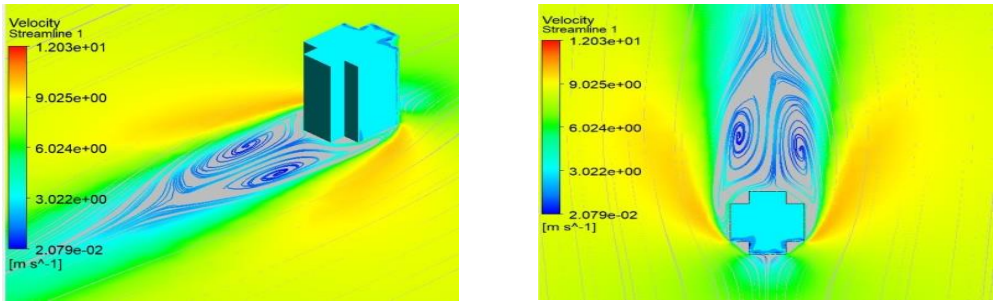

Figure 33: Horizontal and Vertical Streamlines for 0 degree wind inclination

4.3 VELOCITY STREAMLINES

In ANSYS CFD simulations, velocity streamlines play a crucial role in analysing fluid flow patterns and providing valuable insights into the behaviour of the fluid. The concept of velocity streamlines is based on the fundamental principle of conservation of mass and provides a visual representation of the direction and magnitude of the fluid velocity at every point within the computational domain.

Velocity streamlines are continuous curves that are tangent to the local velocity vector at each point. They provide a clear depiction of the flow field, illustrating how the

fluid moves through space and interacts with the boundaries and obstacles within the simulation domain. By observing the velocity streamlines, engineers and researchers can gain a deeper understanding of the flow behaviour, identify regions of recirculation, turbulence, or separation, and evaluate the overall efficiency of a design.

One of the primary benefits of velocity streamlines in ANSYS CFD simulations is their ability to reveal information about flow patterns that may not be easily discernible from other data representations. By tracing the streamlines, engineers can observe the direction of flow at any given point and identify regions of flow convergence or divergence. This information can be particularly useful in analysing the performance of various components, optimizing designs, and predicting the behaviour of fluid systems.

Furthermore, velocity streamlines can help identify areas of high velocity gradients or velocity shear, which can be critical in assessing the potential for turbulence or boundary layer separation. These insights can guide the design of aerodynamic surfaces, heat exchangers, or other flow-related systems to ensure efficient and reliable performance. By visualizing the streamlines in different planes or sections of the computational domain, engineers can also identify regions of interest and gain a comprehensive understanding of the three-dimensional flow behaviour.

CHAPTER 5

NUMERICAL SIMULATION OF MODEL 2

5.1 MODEL DESCRIPTION

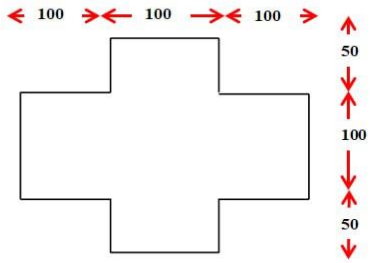

Figure 34: Geometry of Model 2

The model has an area similar to previous model 1 the base dimension is varied by 50mm to analyse the effect of wind pressure. The pressure contours and streamline result of the model are shown below.

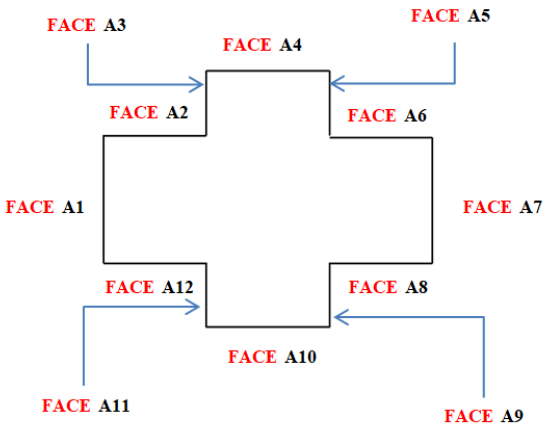

Figure 35: Naming of Faces for Model 2

5.2 PRESSURE CONTOURS

In ANSYS' CFX mode, pressure contours are obtained after analysis. Pressure contours are used to show how the pressure values on a surface vary over time. The pressure contours below demonstrate the relative difference in pressure effect at wind inclination ranging from 0 to 180 degrees at a 30^0degree interval. The pressure contours obtained lead to the following deductions.

1. **When wind angle is 0°**

The range of average pressure values for the wind inclination angle of 0^0 is between **[**-24.25, 28.28]. The maximum positive and negative pressure values of 28.28 and -24.25, respectively, occur on Face A1 and A9. The maximum positive and negative values of 0.46 and -0.40 occur on Face A1 and A9.

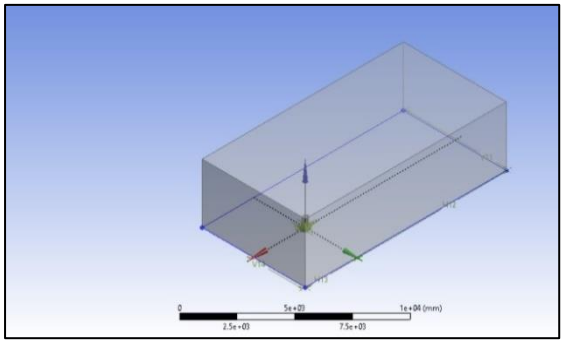

Wind Angle 0 degree				
Faces	Range of pressure	Average pressure	Range of Cp	Average Cp
A1	(-30.90,50.45)	28.28	(-0.50,0.82)	0.46
A2	(-37.47,15.49)	-13.58	(-0.61,0.25)	-0.22
A3	(-30.07,40.58)	-4.96	(-0.49,0.66)	-0.08
A4	(-59.75,3.51)	-21.20	(-0.98,0.06)	-0.34
A5	(-38.22,10.3)	-17.32	(-0.62,0.17)	-0.28
A6	(-24.31,-5.49)	-16.47	(-0.4,-0.09)	-0.26
A7	(-31.6,39.08)	-8.10	(-0.52,0.64)	-0.13
A8	(-23.78,-6.39)	-17.25	(-0.39,-0.1)	-0.28
A9	(-59.6,-0.44)	-24.25	(-0.97,-0.01)	-0.40
A10	(-21.32,-13.97)	-18.57	(-0.35,-0.23)	-0.30
A11	(-22.74,-15.45)	-19.29	(-0.37,-0.25)	-0.31
A12	(-21.30,-6.75)	-16.31	(-0.35,-0.11)	-0.27

Figure 36: Geometry and Pressure and Cp values

Table 8: Pressure contour of faces at 0-degree wind inclination

Face A1	Face A2	Face A3	Face A4	Face A5	Face A6
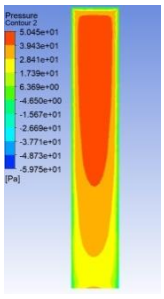	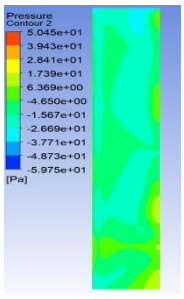	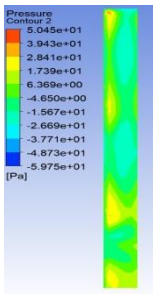	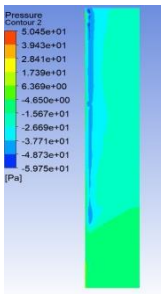	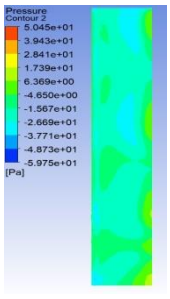	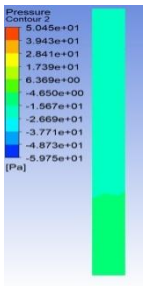

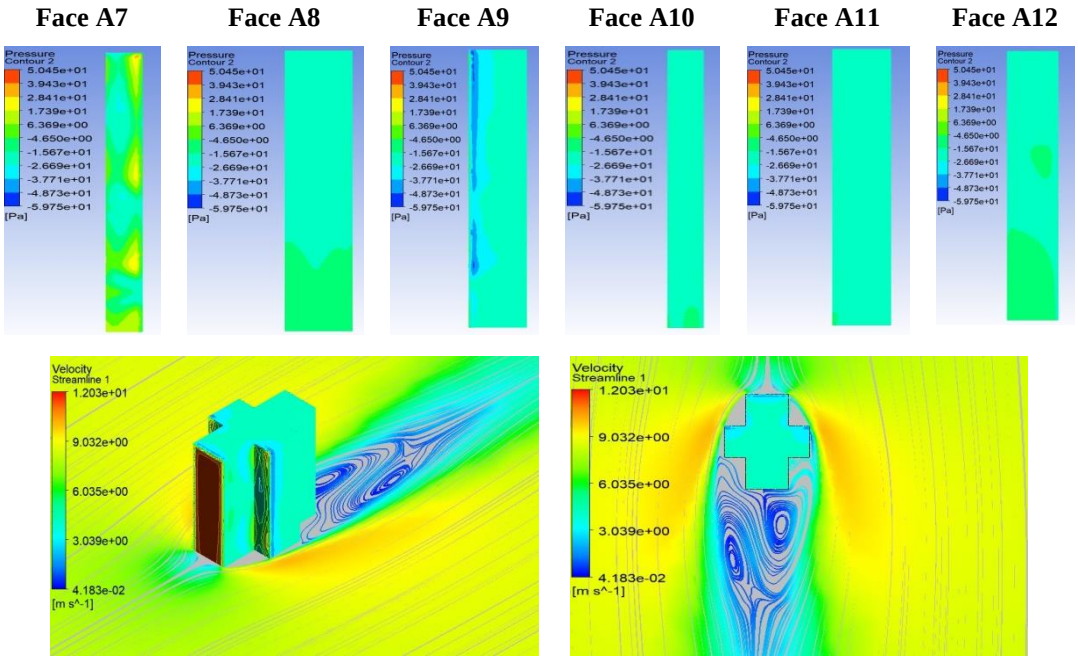

Figure 37: Horizontal and Vertical Streamlines for 0 degree wind inclination

2. When wind angle is 30°

The range of average pressure values for the wind inclination angle of 30^0 is between [-31.08, 33.22]. The maximum positive and negative pressure values of 33.22 and -31.08, respectively, occur on Face A2 and A4. The range of pressure coefficient Cp lies in the range ε [-0.51, 0.54]. The maximum positive and negative values of 0.54 and -0.51 occur on Face A2 and A4, indicating the areas of the building that will experience the highest wind load.

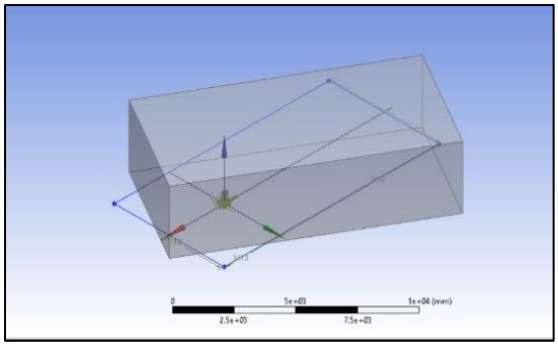

Wind Angle 30 degree				
Faces	Range of pressure	Average pressure	Range of Cp	Average Cp
A1	(-43.95,50.07)	21.99	(-0.72,0.82)	0.36
A2	(-82.90,46.20)	33.22	(-82.90,46.20)	0.54
A3	(-90.60,46.80)	26.63	(-1.48,0.76)	0.43
A4	(-66.60,-1.90)	-31.08	(-1.09,-0.03)	-0.51
A5	(-50.20-7.34)	-22.82	(-0.82,-0.12)	-0.37
A6	(-63.30,-16.80)	-30.83	(-1.03,-0.27)	-0.50
A7	(-30.60,-8.66)	-21.58	(-0.50,-0.14)	-0.35
A8	(-46.00,-3.77)	-27.15	(-0.75,-0.06)	-0.44
A9	(-28.60,3.60)	-18.21	(-0.47,-0.06)	-0.30
A10	(-23.50,-2.19)	-16.07	(-0.38,-0.04)	-0.26
A11	(-25.90,-2.30)	-16.41	(-0.42,-0.04)	-0.27
A12	(-30.70,-2.30)	-17.74	(-0.50,-0.04)	-0.29

Figure 38: Geometry and Pressure and Cp values

Table 9: Pressure contour of faces at 30-degree wind inclination

Face A1 **Face A2** **Face A3** **Face A4** **Face A5** **Face A6**

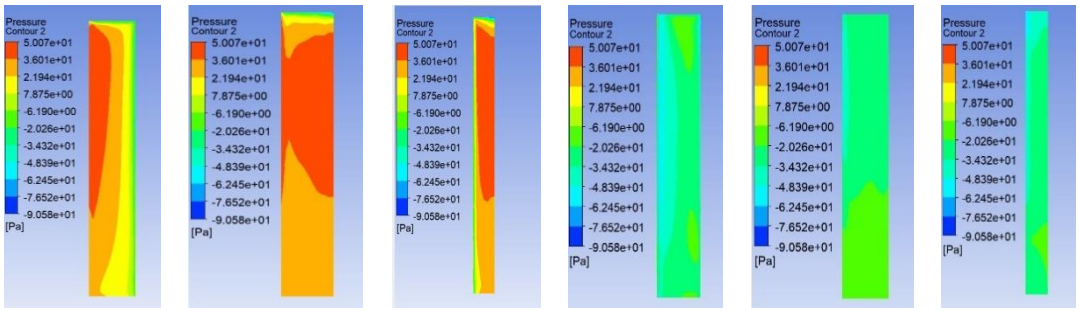

Face A7 **Face A8** **Face A9** **Face A10** **Face A11** **Face A12**

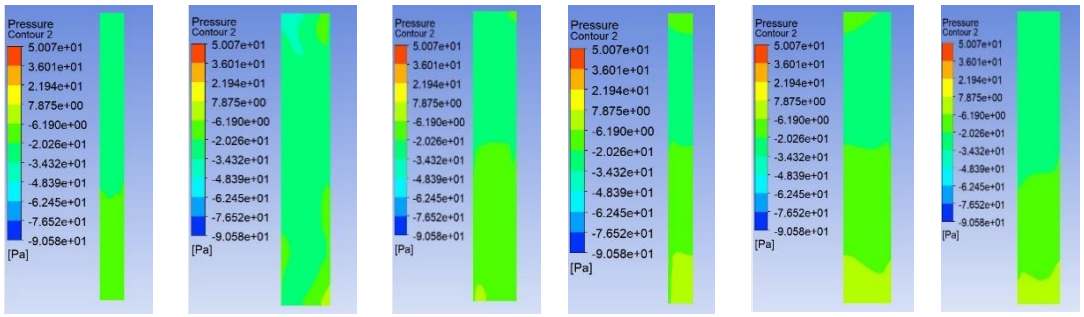

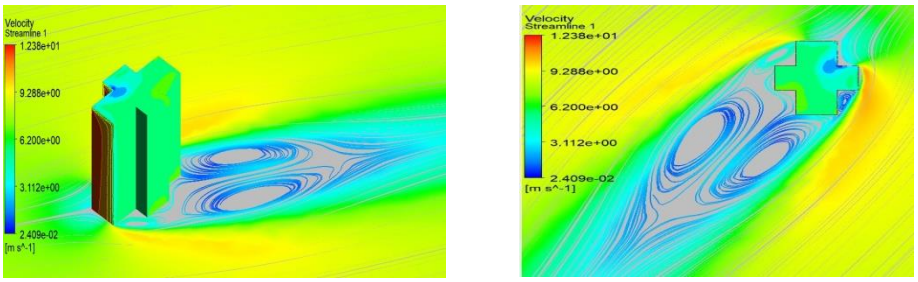

Figure 39: Horizontal and Vertical Streamlines for 0 degree wind inclination

3. When wind angle is 60°

The range of average pressure values for the wind inclination angle of 60^0 is between [-23.86, 38.30]. The maximum positive and negative pressure values of 38.30 and -23.86, respectively, occur on Face A3 and A12. The range of pressure coefficient Cp lies in the range ε [-0.39, 0.63]. The maximum positive and negative values of 0.63 and -0.39 occur on Face A3 and A12, indicating the areas of the building that will experience the highest wind load.

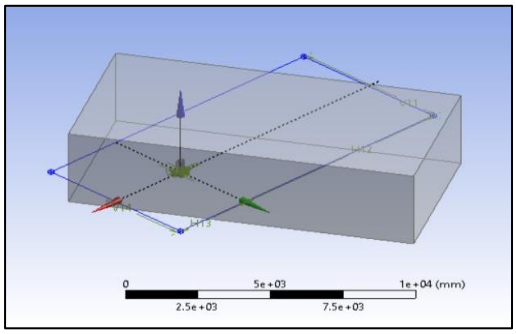

Wind Angle 60 degree				
Faces	Range of pressure	Average pressure	Range of Cp	Average Cp
A1	(-56.53,5.62)	-20.96	(-0.92,0.09)	-0.34
A2	(-45.30,48.60)	33.89	(-0.74,0.79)	0.55
A3	(-46.40,49.10)	38.30	(-0.76,0.80)	0.63
A4	(-34.00,46.10)	21.76	(-0.56,0.75)	0.36
A5	(-40.30,-4.50)	-19.42	(-0.66,-0.07)	-0.32
A6	(-36.10,7.77)	-9.40	(-0.59,0.13)	-0.15
A7	(-33.00,-7.95)	-20.44	(-0.54,-0.13)	-0.33
A8	(-33.30,22.80)	-3.55	(-0.54,0.37)	-0.06
A9	(-32.00,-3.35)	-18.17	(-0.52,-0.05)	-0.30
A10	(-27.40,-4.78)	-18.48	(-0.45,-0.08)	-0.30
A11	(-29.80,-4.69)	-18.76	(-0.49,-0.08)	-0.31
A12	(-46.30,-10.40)	-23.86	(-0.76,-0.17)	-0.39

Figure 40: Geometry and Pressure and Cp values

Table 10: Pressure contour of faces at 60-degree wind inclination

Face A1	Face A2	Face A3	Face A4	Face A5	Face A6
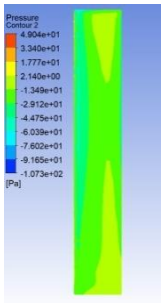	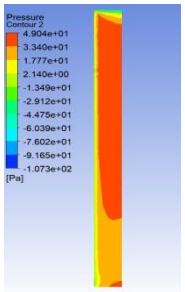	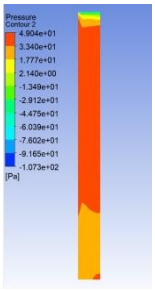	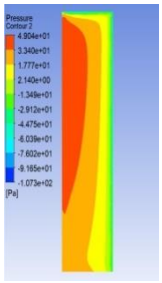	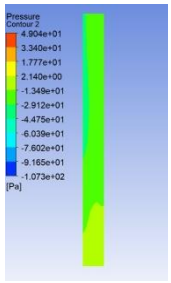	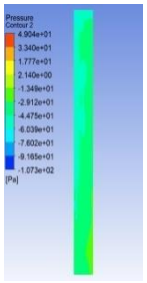
Face A7	**Face A8**	**Face A9**	**Face A10**	**Face A11**	**Face A12**
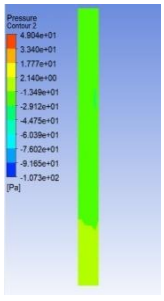	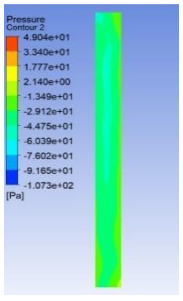	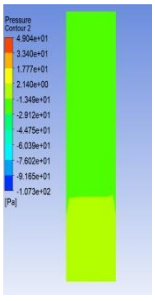	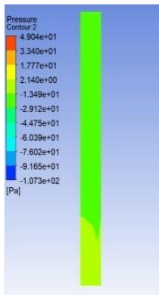	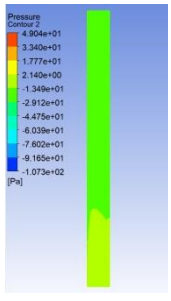	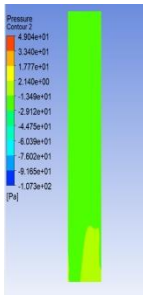

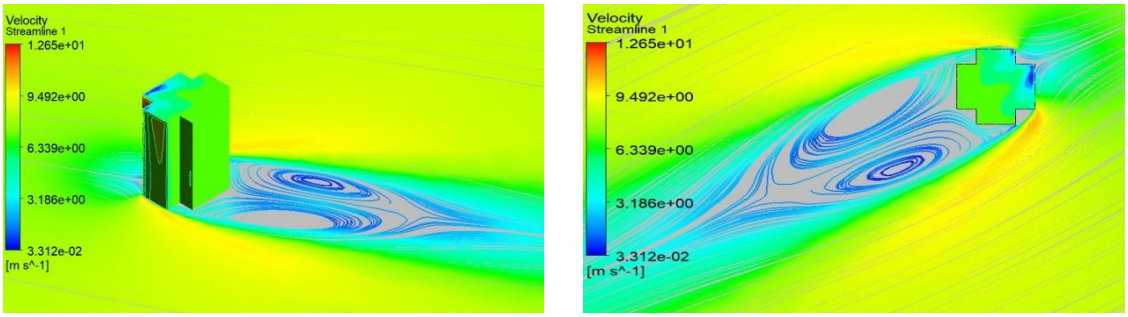

Figure 41: Horizontal and Vertical Streamlines for 0 degree wind inclination

4. When wind angle is 90°

The range of average pressure values for the wind inclination angle of 90^0 is between [-24.24, 36.39]. The maximum positive and negative pressure values of 36.39 and -24.24, respectively, occur on Face A4 and A1. The range of pressure coefficient Cp lies in the range ε [-0.40, 0.59]. The maximum positive and negative values of 0.59 and -0.40 occur on Face A4 and A1.

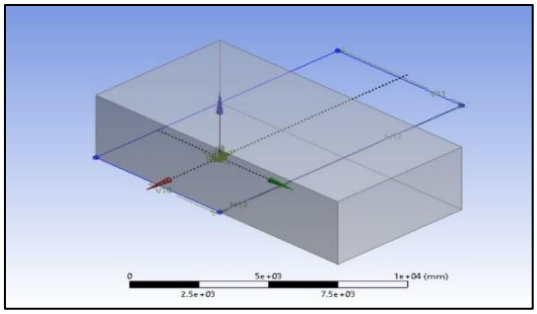

Wind Angle 90 degree				
Faces	Range of pressure	Average pressure	Range of Cp	Average Cp
A1	(-47.89,-10.20)	-24.24	(-0.78,-0.17)	-0.40
A2	(-39.80,44.10)	23.39	(-0.65,0.72)	0.38
A3	(-47.60,38.50)	25.11	(-0.78,0.63)	0.41
A4	(-36.90,48.70)	36.39	(-0.60,0.80)	0.59
A5	(-29.60,-8.28)	-20.41	(-0.48,-0.14)	-0.33
A6	(-42.60,39.40)	26.61	(-0.70,0.64)	0.43
A7	(-28.00,-10.40)	-21.54	(-0.46,-0.17)	-0.35
A8	(-36.44,44.70)	25.08	(-0.59-0.73)	0.41
A9	(-27.70,-5.38)	-18.55	(-0.45,-0.09)	-0.30
A10	(-24.70,-5.88)	-16.91	(-0.40,-0.10)	-0.28
A11	(-24.20,-4.60)	-16.18	(-0.40,-0.08)	-0.26
A12	(-40.90,-5.31)	-19.31	(-0.67,-0.09)	-0.32

Figure 42: Geometry and Pressure and Cp values

Table 11: Pressure contour of faces at 90-degree wind inclination

Face A1	Face A2	Face A3	Face A4	Face A5	Face A6
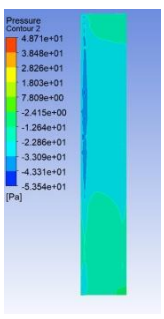	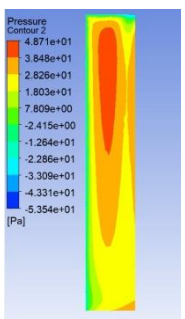	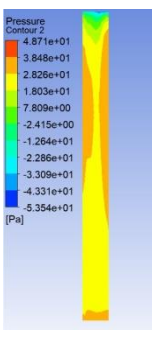	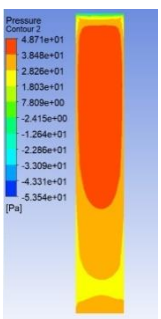	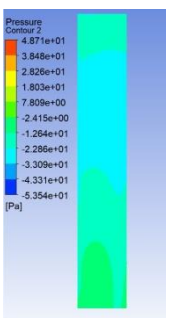	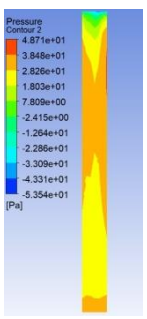

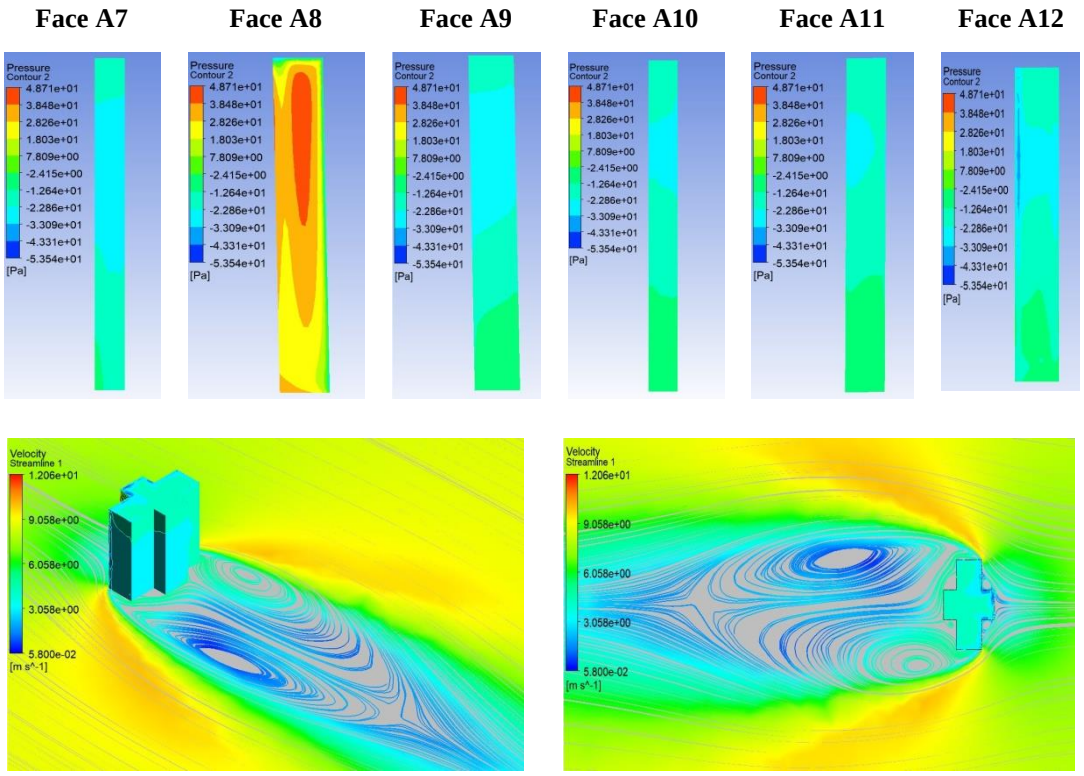

Figure 43: Horizontal and Vertical Streamlines for 0 degree wind inclination

5. When wind angle is 120°

The range of average pressure values for the wind inclination angle of 120^0 is between [-24.65, 38.48]. The maximum positive and negative pressure values of 38.48 and -24.65, respectively, occur on Face A6 and A1. The range of pressure coefficient Cp lies in the range ε [-0.40, 0.63]. The maximum positive and negative values of 0.63 and -0.40 occur on Face A6 and A1, indicating the areas of the building that will experience the highest wind load.

Table 12: Pressure contour of faces at 120-degree wind inclination

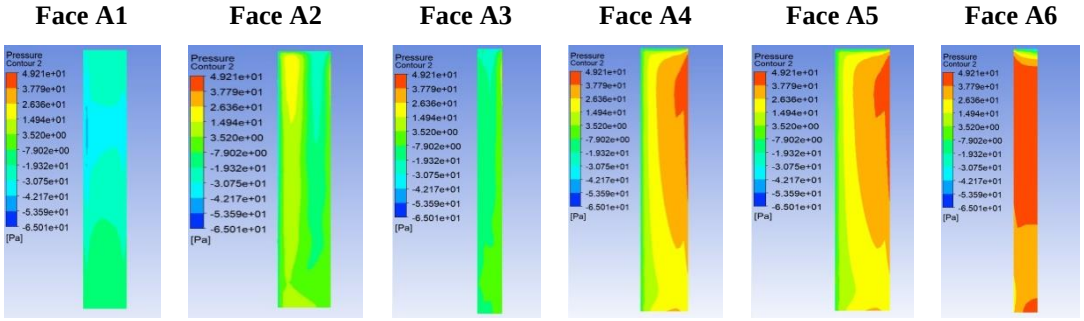

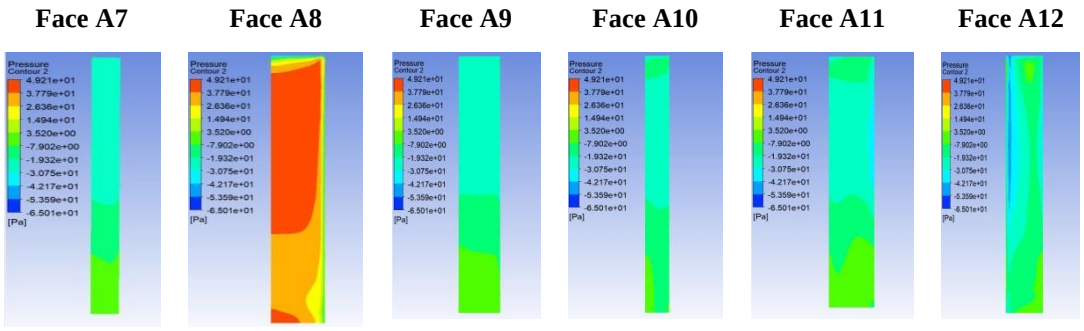

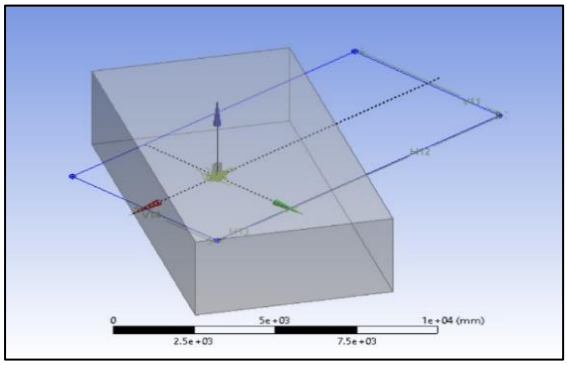

Wind Angle 120 degree				
Faces	Range of pressure	Average pressure	Range of Cp	Average Cp
A1	(-45.76,-11.73)	-24.65	(-0.75,-0.19)	-0.40
A2	(-35.12,22.14)	-4.05	(-0.57,0.36)	-0.07
A3	(-39.58,7.08)	-9.74	(-0.65,0.12)	-0.16
A4	(-27.47,46.13)	21.59	(-0.45,0.75)	0.35
A5	(-31.70,-4.21)	-18.95	(-0.52,-0.07)	-0.31
A6	(-45.16,49.21)	38.48	(-0.74,0.80)	0.63
A7	(-28.49,-3.98)	-18.19	(-0.47,0.06)	-0.30
A8	(-45.16,48.67)	33.98	(-0.74,0.79)	0.55
A9	(-29.35,-2.53)	-17.55	(-0.48,-0.04)	-0.29
A10	(-30.04,-5.36)	-18.71	(-0.49,-0.09)	-0.31
A11	(-40.87,-2.78)	-18.16	(-0.67,-0.05)	-0.30
A12	(-56.19,3.57)	-20.42	(-0.92,0.06)	-0.33

Figure 44: Geometry and Pressure and Cp values

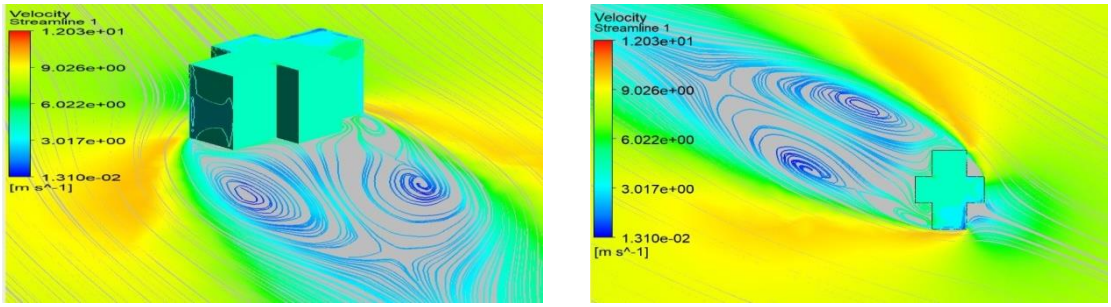

Figure 45: Horizontal and Vertical Streamlines for 0 degree wind inclination

6. When wind angle is 150°

The range of average pressure values for the wind inclination angle of 150^0 is between [-31.91, 32.94]. The maximum positive and negative pressure values of 32.94 and -31.91, respectively, occur on Face A8 and A4. The maximum positive and negative values of 0.54 and -0.52 occur on Face A8 and A4

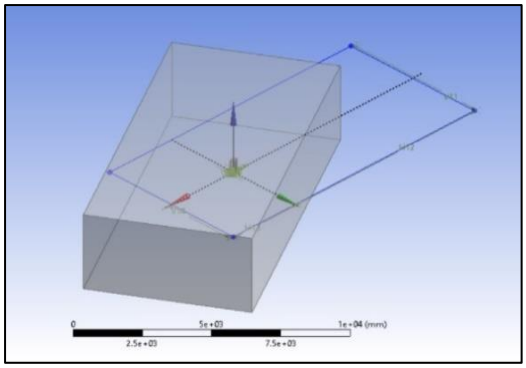

Wind Angle 150 degree				
Faces	Range of pressure	Average pressure	Range of Cp	Average Cp
A1	(-33.75,-4.42)	-17.88	(-0.55,-0.07)	-0.29
A2	(-44.80,-6.04)	-27.71	(-0.73,-0.10)	-0.45
A3	(-63.48,-16.93)	-31.56	(-1.04,-0.28)	-0.52
A4	(-67.72,-3.13)	-31.91	(-1.11,-0.05)	-0.52
A5	(-26.96,-4.11)	-16.36	(-0.44,-0.07)	-0.27
A6	(-103.75,46.78)	26.29	(-1.69,0.76)	0.43
A7	(-24.48,-3.90)	-16.12	(-0.40,-0.06)	-0.26
A8	(-89.59,46.25)	32.94	(-1.46,0.76)	0.54
A9	(-27.19,-8.24)	-18.96	(-0.44,-0.13)	-0.31
A10	(-28.85,-11.94)	-20.80	(-0.47,-0.19)	-0.34
A11	(-45.47,-9.47)	-22.10	(-0.74,-0.15)	-0.36
A12	(-43.80,50.22)	21.80	(-0.72,0.82)	0.36

Figure 46: Geometry and Pressure and Cp values

Table 13: Pressure contour of faces at 150-degree wind inclination

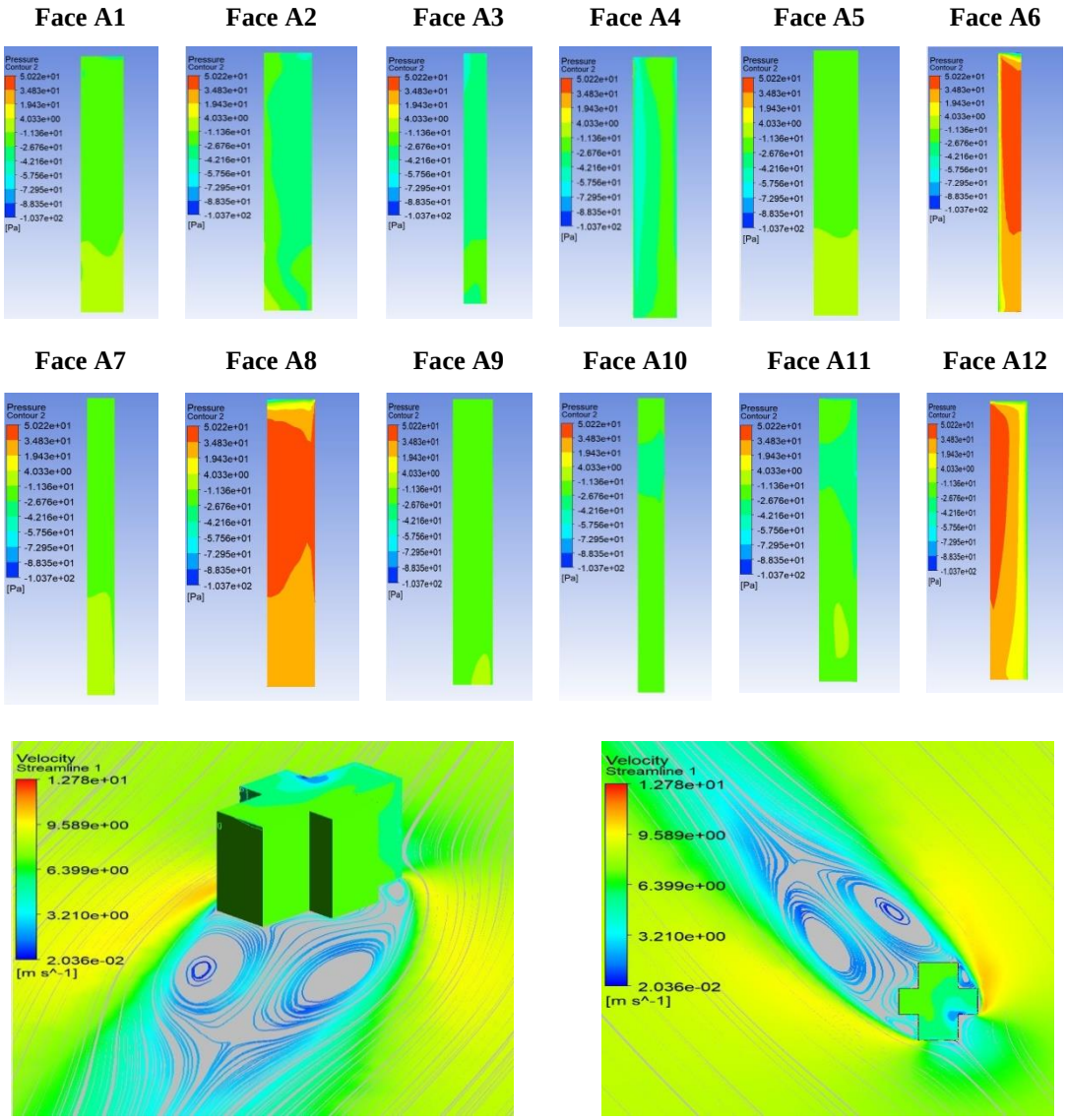

Figure 47: Horizontal and Vertical Streamlines for 0 degree wind inclination

7. When wind angle is 180°

The range of average pressure values for the wind inclination angle of 180^0 is between [-23.64, 28.48]. The maximum positive and negative pressure values of 28.48 and -23.64, respectively, occur on Face A12 and A4. The range of pressure coefficient Cp lies in the range ε [-0.39, 0.46]. The maximum positive and negative values of 0.46 and -0.39 occur on Face A12 and A4.

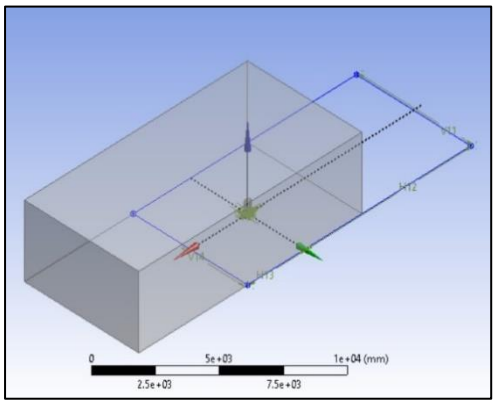

Wind Angle 180 degree				
Faces	Range of pressure	Average pressure	Range of Cp	Average Cp
A1	(-21.50,-6.03)	-16.05	(-0.35,-0.10)	-0.26
A2	(-22.61,-15.41)	-18.99	(-0.37,-0.25)	-0.31
A3	(-21.20,-13.99)	-18.34	(-0.35,-0.23)	-0.30
A4	(-61.48,-2.34)	-23.64	(-1.00,-0.04)	-0.39
A5	(-24.09,-7.00)	-17.29	(-0.39,-0.11)	-0.28
A6	(-32.45,40.71)	-7.72	(-0.53,0.66)	-0.13
A7	(-25.08,-5.44)	-16.64	(-0.41,-0.09)	-0.27
A8	(-37.73,11.90)	-16.89	(-0.62,0.19)	-0.28
A9	(-60.80,3.09)	-21.88	(-0.99,0.05)	-0.36
A10	(-29..88,40.89)	5.50	(-0.49,0.67)	-0.09
A11	(-37.80,15.58)	-14.01	(-0.62,0.25)	-0.23
A12	(-32.95,50.36)	28.48	(-0.54,0.82)	0.46

Figure 48: Geometry and Pressure and Cp values

Table 14: Pressure contour of faces at 180-degree wind inclination

Face A1	Face A2	Face A3	Face A4	Face A5	Face A6
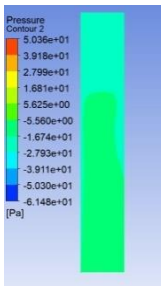	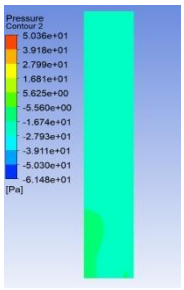	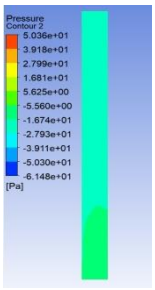	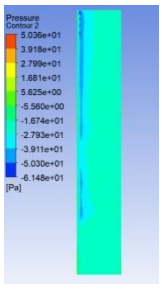	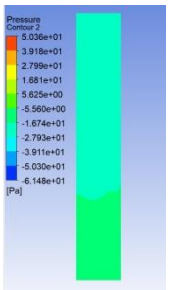	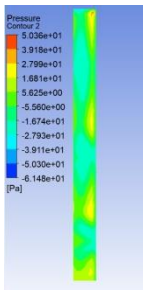
Face A7	**Face A8**	**Face A9**	**Face A10**	**Face A11**	**Face A12**
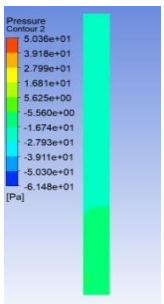	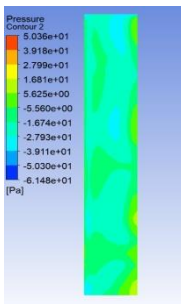	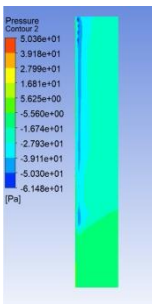	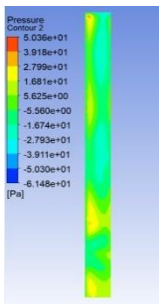	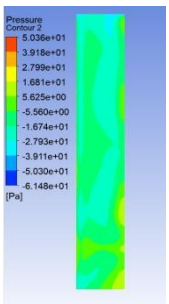	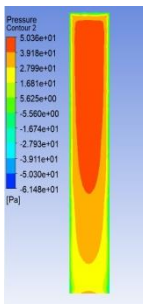

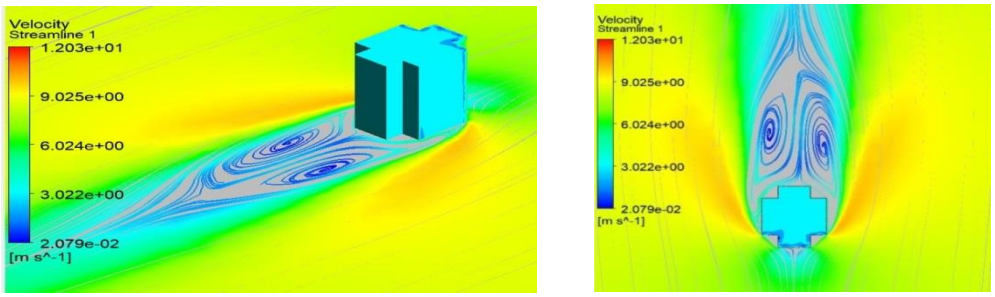

Figure 49: Horizontal and Vertical Streamlines for 0 degree wind inclination

CHAPTER 6

DESIGN AND VALIDATION OF MODEL

To ensure the accuracy and reliability of the findings, a distinct reference model called Model X was created and subjected to thorough analysis. The design of Model X was meticulously crafted to consist of a single square cross-section, measuring 200 mm by 200mm, uniformly maintained throughout its height, which spans 60 meters. It is compared with the acceptable values as given in international standards international standards and the graphical representation of the same is plotted in **Figure 30**.

From **Table 3**, it may be observed that Cp values for faces A, B, C and D are varying and the errors are within the allowable limit. Cp values are used to describe the distribution of pressure over a surface, and they are calculated as the ratio of the pressure difference between the surface and the free stream velocity, to the dynamic pressure of the free stream. The Cp values for each face of Square model (A, B, C, and D) and the percentage variation of Cp values for each face has been recorded in **Table 5**. This suggests that the performance of Square model is satisfactory with respect to its response to wind loading, and the Cp values can be used to design and optimize the structure further.

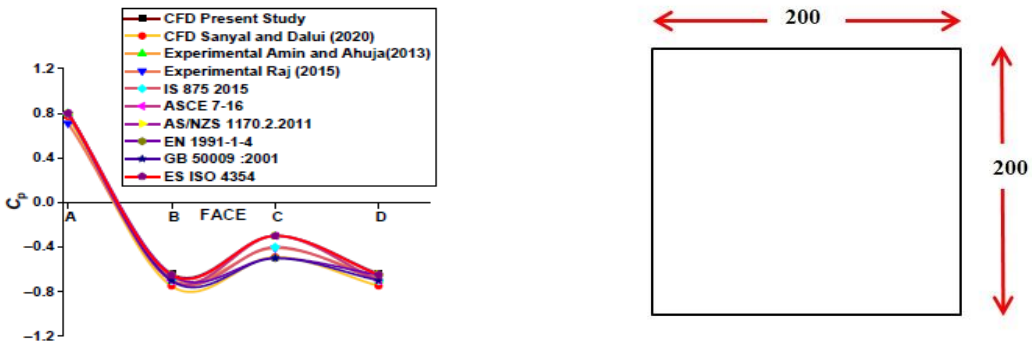

Figure 50: Average Cp for Model X and Geometry of Square Model X

Table 15: Comparing Cp values of Model X with acceptable Cp values in accordance to IS: 875 (Part III) – 2015

Coefficient of Pressure, Cp	Faces of Sqaure Model			
	A	B	C	D
According to IS: 875 (Part III) – 2015	0.8	-0.25	-0.8	-0.8
Square Model	0.63	-0.66	-0.48	-0.40

Table 16: Validation with International Standards

0 deg												
Wind -Direction	**Faces**	**Simulation**	**Sanyal**	**Raj 2015**	**IS: 875**	**ASCE**	**AS/NZS**	**EN1991**	**BS6399**	**GB50009**	**NSCP**	**ES/ISO**
Wind- ward Side	A	0.63	0.8	0.71	0.8	0.8	0.8	0.8	0.76	0.8	0.8	0.8
Lee-ward Side	C	-0.48	-0.5	-0.67	-0.25	-0.5	-0.5	-0.55	-0.5	-0.5	-0.5	-0.65
Side walls	B & D	-0.53	-0.7	-0.41	-0.8	-0.7	-0.65	-0.8	-0.8	-0.7	-0.7	-0.7
90 deg												
Wind- ward Side	A	0.67	0.8	0.73	0.8	0.8	0.8	0.8	0.76	0.8	0.8	0.8
Lee-ward Side	C	-0.43	-0.5	-0.66	-0.25	-0.5	-0.5	-0.55	-0.5	-0.5	-0.5	-0.65
Side walls	B & D	-0.53	-0.7	-0.42	-0.8	-0.7	-0.65	-0.8	-0.8	-0.7	-0.7	-0.7

Table 17: Results for Square Model

Square Model 0 deg				
Face	**Range of Presure**	**Average value of Pressure**	**Range of Cp**	**Average Value of Cp**
A	(-49.55,49.14)	27.10	(-0.81,0.80)	0.63
B	(-54.48,0.21)	-24.83	(-0.89,0.0)	-0.66
C	(-35.32,-3.89)	-17.80	(-0.58,-0.06)	-0.48
D	(-44.17,-10.03)	-24.29	(-0.72,-0.16)	-0.40
Square Model 90 deg				
Face	**Range of Presure**	**Average value of Pressure**	**Range of Cp**	**Average Value of Cp**
A	(-44.98,-10.79)	-24.18	(-0.73,-0.18)	0.67
B	(-45.71,49.22)	27.32	(-0.75,0.80)	-0.65
C	(-52.84,-11.84)	-25.21	(-0.86,-0.18)	-0.43
D	(-37.19,-4.68)	-17.78	(-0.08,-0.61)	-0.40

Table 18: Pressure contours for Model X

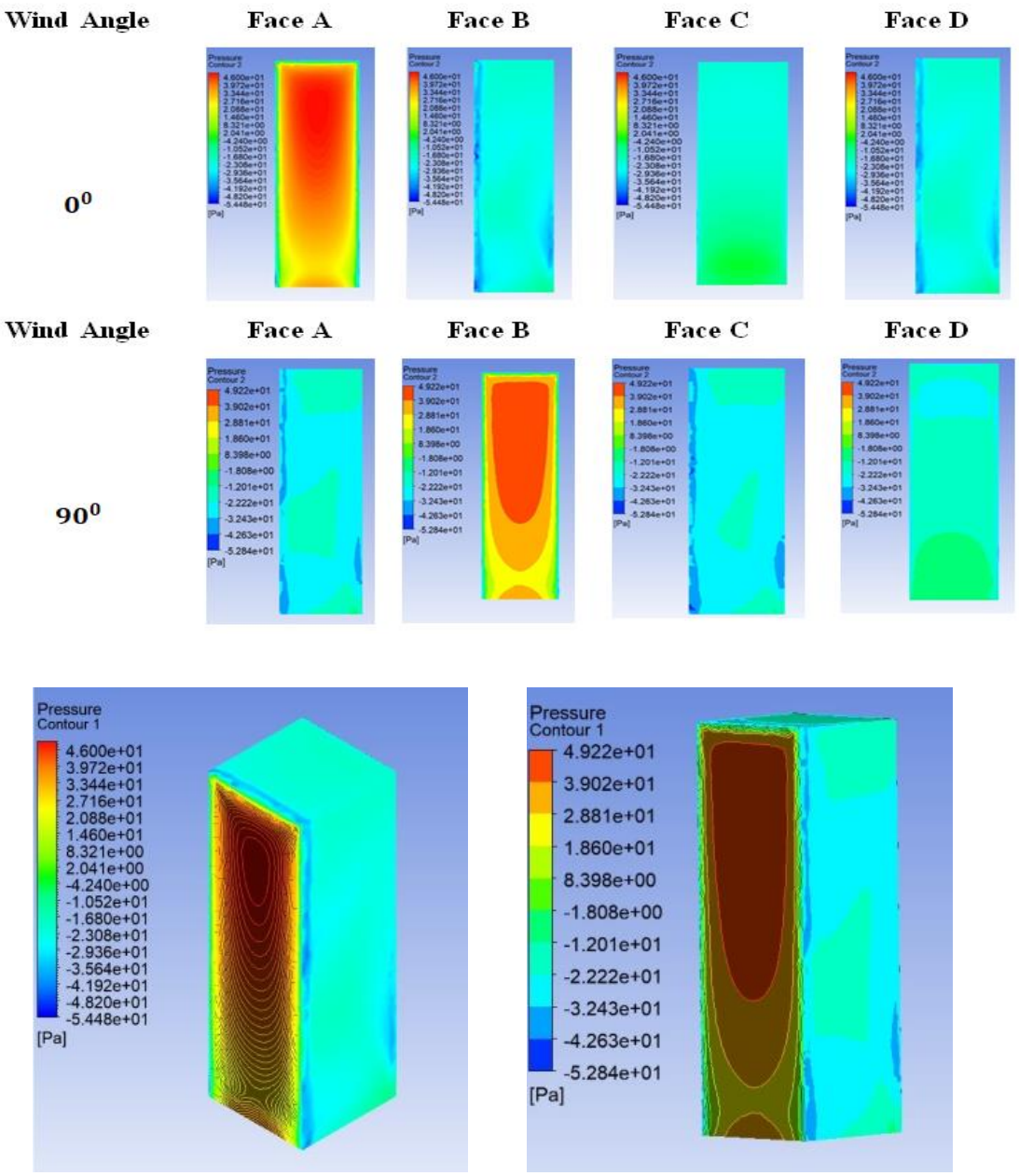

Figure 51: Pressure contour of Model X for 0 and 90 degree

6.1 DRAG AND LIFT FORCES AND MOMENTS

The formulas for calculating the coefficients Cfx, Cfy, Cmx, and Cmy are as follows:

$$Cfx = Fx / (0.5 * \pi * U\text{^}2 * h * A)$$

$$Cfy = Fy / (0.5 * \pi * U\text{^}2 * h * A)$$

$$Cmx = Mx / (0.5 * \pi * U\text{^}2 * h * Ab)$$

$$Cmy = My / (0.5 * \pi * U\text{^}2 * h * Ab)$$

In these equations, Fx and Fy represent the forces, Mx and My represent the moments, U is the flow velocity, h is the reference height, A is the reference area, and Ab is the reference base area. After analysing the graphs depicting the Cfx, Cfy, Cmx, and Cmy values for different wind incidence angles (0^0 to 180^0 at an interval of 30^0), several conclusions can be drawn. Firstly, the moment drags for both **Model 1** and **Model 2** exhibit remarkably similar curves, indicating the accuracy of the obtained results. Secondly, when the wind incidence angle is 90 degree, **Model 2** experiences the highest drag force, whereas the lowest drag force for **Model 2** occurs at a wind incidence angle of 60 degree. Lastly, the maximum lift force for **Model A** is observed at a wind incidence angle of 60 degree, while for **Model A**, it is at angles between 60 and 90 degree.

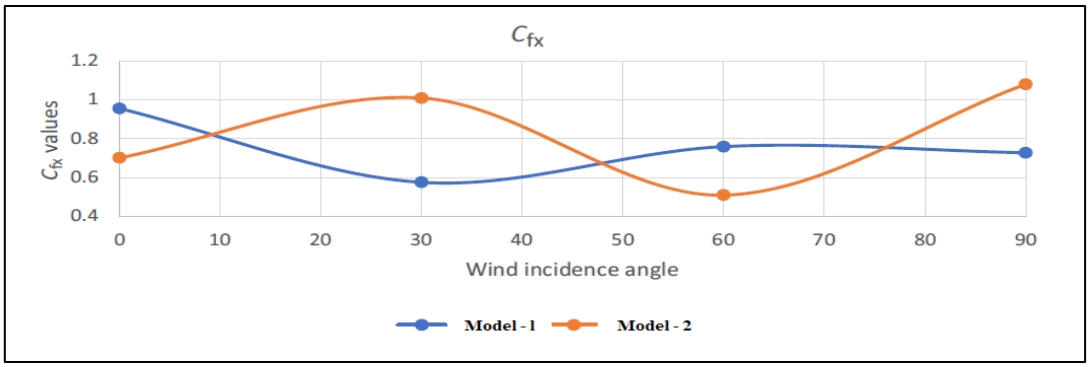

Figure 52: Cfx graph for Model 1 and Model 2

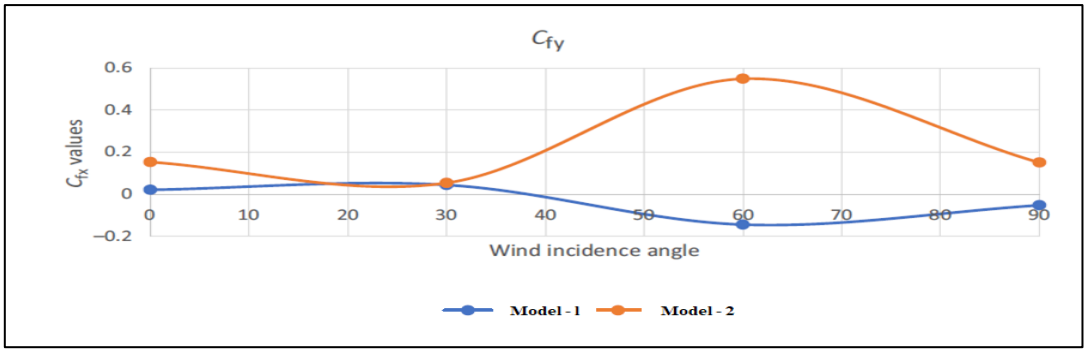

Figure 53: Cfy graph for Model 1 and Model 2

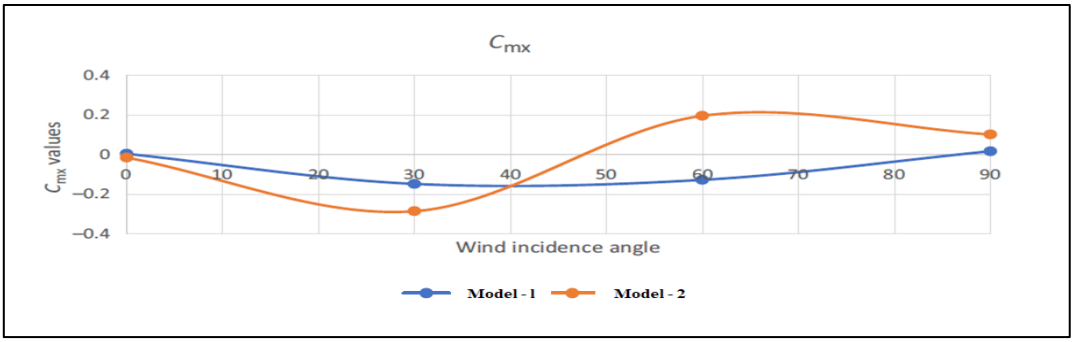

Figure 54: Cmx graph for Model 1 and Model 2

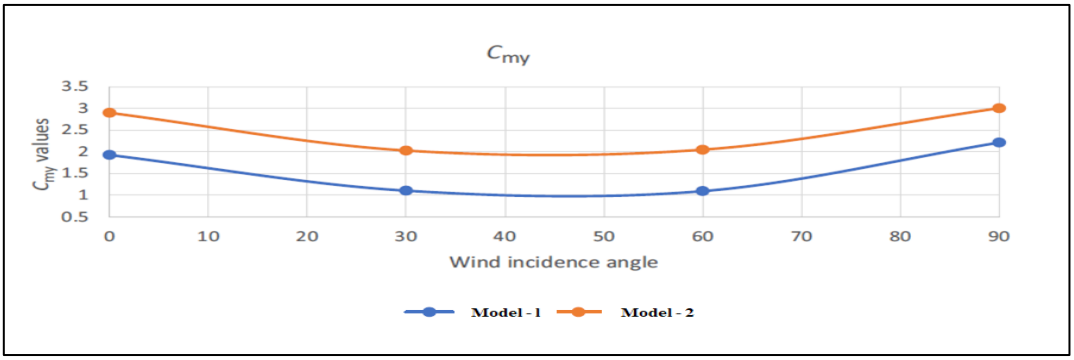

Figure 55: Cmy graph for Model 1 and Model 2

Based on the analysis of the graphs representing wind incidence angles for Model A and Model B, these conclusions can be drawn;

1) The moment drags for both models exhibit similar curves, indicating the accuracy of the results obtained.
2) Model B experiences the highest drag force at a wind incidence angle of 90 degree, while the lowest drag force occurs at an angle of 60 degree for the same model.

3) The lift force is maximized for Model B at a wind incidence angle of 60 degree, whereas Model A demonstrates the minimum lift force between 60 and 90 degrees.

These findings suggest that specific wind incidence angles result in maximum or minimum drag force, as well as lift force, which can lead to the observation of critical faces mentioned in the pressure contours subsection. Consequently, it is important to incorporate appropriate design precautions, such as the provision of windows, when constructing tall buildings to account for these angles.

CHAPTER 7

CONCLUSION

This study examines how wind loads affect tall structures with various corner forms. The study uses ANSYS CFX numerical simulation at a scale of 1:200 using a k-turbulence model. The correctness of the numerical simulation is ensured by comparison of the average face pressure coefficient (Cp) with international standards and experimental research. The outcomes demonstrate the streamlines at different wind incidence angles, allowing for a thorough comprehension of the wind flow patterns. After running a simulation, comparisons between several cross-sectional tall structures of various forms were done. The models employed met IS 875 (Part 3) requirements and had been verified.

The size and form of the building's face have little impact on the pressure distribution, according to an analysis of pressure contours. Additionally, it was noted that in both models, the pressure on the windward face A2 was lower than on the leeward face. Similarities might be seen in the pressure distribution on the lateral faces and the leeward face. Additionally, there were small modifications in the pressure distribution along the models' edges. The horizontal streamlines showed that Face A1 of Model 1 and Mode 2 both showed the largest production of vortices at 0 and 90 degrees.

It was possible to determine the critical faces for different wind incidence angles by comparing the graphs of drag force, drag moment, lift force, and lift moment. Designing tall structures with square and plus-shaped cross sections should take these particular wind angles into account. Regardless of the cross-sectional form of the structure, the CFD methodology provides a time- and cost-effective alternative to techniques like wind tunnel testing for analysing the influence of wind on tall buildings.

REFERENCES

[1] Hwang, H., & Kim, J. (2005). Prediction of wind loads on a tall building in a complex urban environment using computational fluid dynamics. In Proceedings of the 11th Americas Conference on Wind Engineering (11th ACWE) (pp. 1-10).

[2] Hu, H., & Yuan, X. (2008). CFD prediction of wind loads on a tall building with different turbulence models. In Proceedings of the 14th Americas Conference on Wind Engineering (14th ACWE) (pp. 1-10).

[3] Fattahi, R., Mazaheri, K., & Hangan, H. (2019). Simplified CFD approach for wind load prediction on tall buildings. In Proceedings of the 28th International Ocean and Polar Engineering Conference (28th ISOPE) (pp. 1-7).

[4] Zhao, J., & Cheng, Y. (2019). Investigation of turbulence models for CFD simulations of wind loads on tall buildings. In Proceedings of the XX International Conference on Wind Engineering (XX ICWE) (pp. 1-8).

[5] A. Allsop, "BS EN 1991-1-4 Tall Buildings," in ICE (Institution of Civil Engineers), New Eurocode on Wind Loading. London, UK, 11 May 2009.

[6] ANSYS Inc., "FLUENT 12.0 Theory Guide," 2009.

[7] Building Research Establishment, "Wind around tall buildings, BRE Digest 390," Watford, UK, 1994.

[8] British Standards Institution, "BS 6399-2:1997 Loadings for buildings – Part 2: Code of practice for wind loads." London, UK, 1997.

[9] British Standards Institution, "BS EN 1991-1-4:2005 Euro code 1: Actions on structures – Part 1-4: General actions – Wind actions." London, UK, 2005.

[10] I. P. Castro, "CFD for External Aerodynamics in the Built Environment," The QNET-CFD Network Newsletter - Vol. 2: No. 2 – July 2003, pp 4-7, 2003.

[11] Zhang et al., "Experimental measurements and numerical simulations of particle transport and distribution in ventilated rooms," Atmos. Environ., 2006.

[12] Yoshie, R., Tanaka, S., & Hayashi, Y. (2007). CFD prediction of pedestrian wind environment. Journal of Wind Engineering and Industrial Aerodynamics, 95(10), 1749-1774.

[13] Van Hooff, T., Blocken, B., & Van Heijst, G. J. (2014). Large eddy simulation and Reynolds-averaged Navier-Stokes simulation of counter-gradient diffusion in a slot-ventilated enclosure. Computers & Fluids, 103, 92-105.

[14] Van Hooff, T., Blocken, B., & Van Heijst, G. J. (2013). Evaluation of the concentration decay method for predicting natural ventilation performance in a semi-enclosed stadium using CFD simulations. Building and Environment, 59, 367-377.

[15] Van Hooff, T., Blocken, B., & Toparlar, Y. (2012). Full-scale measurements and analysis of transitional flow in a reduced-scale model of a ventilation system. Building and Environment, 56, 155-166.

[16] Van Hooff, T., Blocken, B., & van Heijst, G. J. (2010). Effect of wind direction and urban surroundings on natural ventilation of a large semi-enclosed stadium. Computers & Fluids, 39(8), 1526-1538.

[17] Van Hooff, T., Blocken, B., & Toparlar, Y. (2010). Coupled urban wind flow and indoor natural ventilation modeling of a large semi-enclosed stadium on high-resolution grids. Environmental Modelling & Software, 25(12), 1888-1901.

[18] Tominaga, Y., Stathopoulos, T., & Murakami, S. (2015). Wind tunnel experiments on cross-ventilation flow with contaminant dispersion in unsheltered and sheltered conditions. Building and Environment, 90, 107-121.

[19] Tominaga, Y., Mochida, A., & Yoshie, R. (2010). Simulation of pollutant dispersion in urban areas—recent advances and challenges. Journal of Environmental Engineering, 136(10), 1101-1118.

[20] Singh, M., Li, Y., & Niu, J. (2015). Computational fluid dynamics modeling of air flow and heat transfer in buildings: A review. Renewable and Sustainable Energy Reviews, 52, 1409-1432.

[21] Natarajan, A., & Perumal, K. (2017). Computational fluid dynamics analysis of natural ventilation in buildings: **A** review. Renewable and Sustainable Energy Reviews, 75, 450-461.

[22] Shanmuganathan, S., & Velraj, R. (2016). Numerical simulation of indoor air flow and heat transfer in buildings: A review. Renewable and Sustainable Energy Reviews, 53, 1563-1577.

[23] Singh, H., Sahoo, P. K., & Reddy, S. K. (2016). CFD analysis of heat transfer in buildings: A comprehensive review. Renewable and Sustainable Energy Reviews, 56, 1271-1293.

[24] Dash, S. K., Patnaik, A., & Vijayan, P. K. (2014). Computational fluid dynamics simulation of indoor air flow and heat transfer in buildings: A review. Renewable and Sustainable Energy Reviews, 34, 642-655.